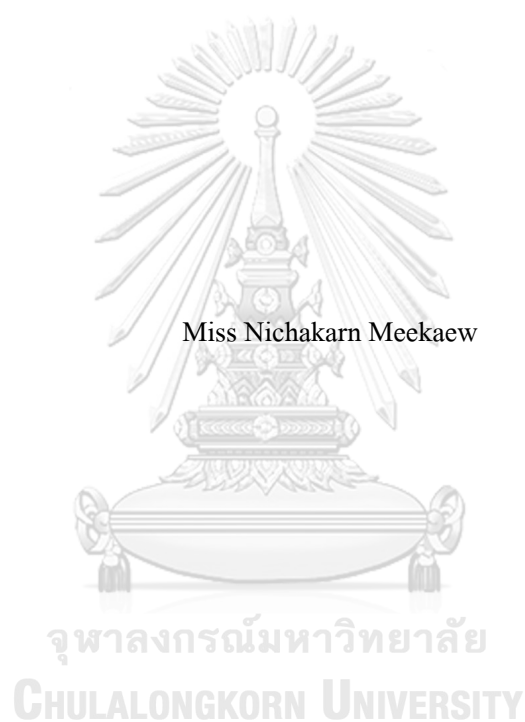


Manganese dioxide coated with tin oxide as cathode material for high-performance aqueous zinc-ion battery.



A Thesis Submitted in Partial Fulfillment of the Requirements  
for the Degree of Master of Engineering in Chemical Engineering

Department of Chemical Engineering

FACULTY OF ENGINEERING

Chulalongkorn University

Academic Year 2021

Copyright of Chulalongkorn University

แมงกานีสไดออกไซด์ที่ถูกเคลือบด้วยชั้นดีบุกออกไซด์เพื่อใช้เป็นวัสดุแคโทดสำหรับแบตเตอรี่  
สังกะสีไอออนแบบน้ำที่มีสมรรถนะสูง



วิทยานิพนธ์นี้เป็นส่วนหนึ่งของการศึกษาตามหลักสูตรปริญญาวิศวกรรมศาสตรมหาบัณฑิต  
สาขาวิชาวิศวกรรมเคมี ภาควิชาวิศวกรรมเคมี  
คณะวิศวกรรมศาสตร์ จุฬาลงกรณ์มหาวิทยาลัย  
ปีการศึกษา 2564  
ลิขสิทธิ์ของจุฬาลงกรณ์มหาวิทยาลัย



ณิกานต์ มีแก้ว : เมงกานีสไดออกไซด์ที่ถูกเคลือบด้วยชั้นดีบุกออกไซด์เพื่อใช้เป็นวัสดุแคโทดสำหรับแบตเตอรี่สังกะสีไอออนแบบน้ำที่มีสมรรถนะสูง. ( Manganese dioxide coated with tin oxide as cathode material for high-performance aqueous zinc-ion battery.) อ.ที่ปรึกษาหลัก : ศ. ดร.อนงค์นาฏ สมหวังธนโรจน์, อ.ที่ปรึกษาร่วม : รศ. ดร.สุรเทพ เขียวหอม

แบตเตอรี่สังกะสี-ไอออนชนิดน้ำแบบชาร์จซ้ำได้ (ZIB) ได้รับความสนใจเพิ่มขึ้นในฐานะเทคโนโลยีกักเก็บพลังงาน เนื่องจากความหนาแน่นของพลังงานสูง, ต้นทุนต่ำ และความเป็นมิตรต่อสิ่งแวดล้อม อย่างไรก็ตามการใช้เมงกานีสไดออกไซด์เป็นแคโทดสำหรับแบตเตอรี่สังกะสี-ไอออนชนิดน้ำ (ZIB) ถูกจำกัดโดยความสามารถในการละลายของเมงกานีสไดออกไซด์ในอิเล็กโทรไลต์ที่เป็นน้ำและการก่อตัวของผลพลอยได้ในระหว่างกระบวนการชาร์จ/การคายประจุ ทำให้ความจุลดลงอย่างรุนแรงและอายุการใช้งานที่จำกัด การปรับเปลี่ยนพื้นผิวเป็นหนึ่งในเทคนิคที่น่าสนใจในการปรับปรุงประสิทธิภาพทางเคมีไฟฟ้าของแบตเตอรี่สังกะสี-ไอออนชนิดน้ำ (ZIB) ในที่นี้เรารายงานว่าฟิล์มดีบุกออกไซด์ ( $\text{SnO}_2$ ) บางเฉียบเป็นอินเทอร์เฟซอิเล็กโทรไลต์ที่เป็นของแข็ง (SEI) เพื่อปรับเปลี่ยนพื้นผิวของเมงกานีสไดออกไซด์ โดยการเคลือบด้วยดีบุกออกไซด์ ( $\text{SnO}_2$ ) บนอิเล็กโทรดเมงกานีสไดออกไซด์ ในที่นี้ได้ทำการเคลือบ ดีบุกออกไซด์ด้วยสัดส่วนที่แตกต่างกันคือ 0.1, 0.2, 0.3 และ 0.4 กรัม ด้วยเหตุนี้แคโทดเมงกานีสไดออกไซด์เคลือบด้วยดีบุกออกไซด์ ได้อิเล็กโทรดที่ดีที่สุดคืออิเล็กโทรดบวก  $0.3\text{MnO}_2@\text{SnO}_2$  จะแสดงค่าความจุที่สูงที่สุด ( $365.37 \text{ mAh/g}@100 \text{ mA/g}$ ) และมีอายุการใช้งานของวงจรที่ดีขึ้นเมื่อเปรียบเทียบกับแคโทดเมงกานีสไดออกไซด์ดั้งเดิม ( $199.02 \text{ mAh/g}@100 \text{ mA/g}$ ) การปรากฏตัวของชั้นดีบุกออกไซด์ ทำหน้าที่เป็นฟิล์มอินเทอร์เฟซอิเล็กโทรไลต์ที่เป็นของแข็ง (SEI) และจากการศึกษาทางจลนศาสตร์ไฟฟ้าเคมีพบว่า การเคลือบดีบุกออกไซด์ ช่วยเพิ่มค่าสัมประสิทธิ์การแพร่ของไอออนสังกะสี, เพิ่มการนำไฟฟ้าได้อย่างมาก งานวิจัยนี้มีส่วนช่วยในการพัฒนาวัสดุแคโทดที่ใช้เมงกานีสไดออกไซด์สำหรับแบตเตอรี่สังกะสี-ไอออนชนิดน้ำแบบชาร์จซ้ำได้ (ZIB) ที่มีประสิทธิภาพสูงและยืดหยุ่น

สาขาวิชา วิศวกรรมเคมี

ปีการศึกษา 2564

ลายมือชื่อนิสิต .....

ลายมือชื่อ อ.ที่ปรึกษาหลัก .....

ลายมือชื่อ อ.ที่ปรึกษาร่วม .....

## 6370105221 : MAJOR CHEMICAL ENGINEERING

KEYWORD:

Nichakarn Meekaew : Manganese dioxide coated with tin oxide as cathode material for high-performance aqueous zinc-ion battery.. Advisor: Prof. ANONGNAT SOMWANGTHANAROJ, Ph.D. Co-advisor: Assoc. Prof. SOORATHEP KHEAWHOM, Ph.D.

Rechargeable aqueous zinc-ion batteries (ZIBs) have attracted increasing attention as an energy storage technology due to their high energy density, low cost, and environmental friendliness. However, the application of manganese dioxide as the cathode for aqueous Zn-ion batteries (ZIBs) is restricted by the solubility of manganese dioxide in aqueous electrolytes and the formation of byproducts during the charge/discharge process, causing severe capacity fading and limited cycle life. Surface modification is one of the interesting techniques to improve zinc-ion batteries electrochemical performance. Here, we report an ultrathin SnO<sub>2</sub> film as an artificial solid electrolyte interphase (SEI) to modify the surface of manganese dioxide by sub-monolayer SnO<sub>2</sub> coating on the electrodes. Here, SnO<sub>2</sub> is coated with different proportions: 0.1, 0.2, 0.3 and 0.4 g. As a result, the SnO<sub>2</sub>-coated MnO<sub>2</sub> cathode yields the best electrode, 0.3MnO<sub>2</sub>@SnO<sub>2</sub> positive electrode. This results in a higher capacity (365.37 mAh/g@100 mA/g) and better cycle life compared with pristine MnO<sub>2</sub> (199.02 mAh/g@100 mA/g). The presence of the SnO<sub>2</sub> layer acts as an artificial cathode electrolyte interface, the electrochemical kinetical studies reveal that the SnO<sub>2</sub> coating greatly improves the diffusion coefficient of zinc ions and investigation reveals the SnO<sub>2</sub> greatly improves the electrical conductivity. This research contributes to the development of MnO<sub>2</sub>-based cathode materials for high-performance and flexible ZIBs.

Field of Study: Chemical Engineering

Student's Signature .....

Academic Year: 2021

Advisor's Signature .....

Co-advisor's Signature .....

## ACKNOWLEDGEMENTS

The author would like to sincerely grateful to her advisor, Professor Anongnat Somwangthanaroj, for her invaluable help and constant encouragement throughout the course of this research. I am most grateful for her teaching and advice, not only the research methodologies but also many other methodologies in life. I would not have achieved this far and this thesis would not have been completed without all the support that I have always received from her.

The author would also be thankful to Associated Professor Soorathep Kheawhom as a co-advisor for instruction about my research practice and inspiring my interest that I should do for the better experiments.

The author would like to extend her grateful thanks to Prof. Tawatchai Charinpanitkul, Dr. Chutimon Satirapipathkul and Assistant Professor Pornchai Bumroongsri as the chairman, committee and external examiner of this thesis, who provided suggestions and recommendations for this research.

Additionally, the author would like to extend her thanks to all members of Associated Professor Soorathep Kheawhom's group Laboratory and Polymer Engineering Laboratory of the Department of Chemical Engineering, Faculty of Engineering, Chulalongkorn University, for their assistance, discussion, and friendly encouragement in solving problems. Especially, Mr. Wathanyu Kaoian and Miss. Natta Jaikrajang.

Finally, my deepest regard is cordially extended to my family and parents, who have always been supporting, loving, understanding as well as encouragement during my master degree study.

Nichakarn Meekaew

## TABLE OF CONTENTS

	<b>Page</b>
.....	iii
ABSTRACT (THAI).....	iii
.....	iv
ABSTRACT (ENGLISH).....	iv
ACKNOWLEDGEMENTS.....	v
TABLE OF CONTENTS.....	vi
LIST OF TABLES.....	ix
LIST OF FIGURES.....	x
CHAPTER 1 INTRODUCTION.....	12
1.1 General Introduction.....	12
1.2 Objective of the research.....	14
1.3 Scope of the research.....	15
CHAPTER 2 THEORY AND LITERATURE REVIEWS.....	16
2.1 Mechanistic study of Zinc-ion battery.....	16
2.1.1 Side reaction: The formation of $\text{ZnSO}_4(\text{OH})_6 \cdot x\text{H}_2\text{O}$ (ZHS).....	17
2.1.2 Dissolution of manganese-based oxide.....	19
2.2 Solid electrolyte interphase (SEI).....	20
2.2.1 Naturally Solid electrolyte interface (SEI).....	20
2.4 Tin oxide, $\text{SnO}_2$ .....	28
2.5 Analytical Techniques.....	30
2.5.1 Cyclic Voltammetry (CV).....	30

2.5.2 Electrochemical Impedance Spectroscopy (EIS).....	31
2.5.3 Galvanostatic charge-discharge Test .....	32
CHAPTER 3            METHODODOLOGY .....	34
3.1 Materials.....	34
3.2 Material Synthesis. ....	34
3.2.1 Synthesis of $\alpha$ -MnO <sub>2</sub> .....	34
3.2.2 Synthesis of $\alpha$ -MnO <sub>2</sub> @SnO <sub>2</sub> .....	34
3.3.1 Coin cell .....	35
3.3.2 Pouch cell.....	36
3.4 Positive Electrode characterizations.....	37
3.4.1 Structural properties.....	37
3.4.2 Morphology.....	37
3.4.3 Chemical composition.....	37
3.5 Electrochemical Techniques .....	37
3.5.1 Battery Performance .....	37
3.5.2 Cyclic voltammetry (CV).....	38
3.5.3 Electrochemical Impedance Spectroscopy (EIS).....	38
3.6 Inductively Coupled Plasma (ICP).....	38
3.7 Methodology .....	39
CHAPTER 4            RESULTS AND DISCUSSION.....	42
4.1 Materials Characterization .....	42
4.2 Electrochemical performance of batteries .....	45
CHAPTER 5            CONCLUSION .....	57
APPENDIX.....	58

REFERENCES .....2

VITA .....5



จุฬาลงกรณ์มหาวิทยาลัย  
**CHULALONGKORN UNIVERSITY**

## LIST OF TABLES

	<b>Page</b>
Table 3.1 Project Planning .....	41



## LIST OF FIGURES

	<b>Page</b>
Figure 2.1 Schematic representation of electrolytic process and structure change process of the aqueous rechargeable Zn/MnO <sub>2</sub> battery in 2M ZnSO <sub>4</sub> + 0.5M MnSO <sub>4</sub> electrolyte.....	16
Figure 2.2 The role of ZHS in the discharge process. [5].....	18
Figure 2.3 The capacitance of MnO <sub>2</sub> electrodes in 2M ZnSO <sub>4</sub> electrolytes after washing in acetate buffer for different times to eliminate ZHS formation. [5].....	18
Figure 2.4 Cycle performances of the Zn/ $\delta$ -MnO <sub>2</sub> cells using different electrolytes.....	19
Figure 2.5 Diffusion coefficient contrast curve of CMO and $\alpha$ -MnO <sub>2</sub> . [9].....	21
Figure 2.6 The galvanostatic discharge comparison curve in 100 mA g <sup>-1</sup> of $\alpha$ -MnO <sub>2</sub> electrode and CMO electrode. [9].....	21
Figure 2.7 Comparison of manganese dissolution rate of $\alpha$ -MnO <sub>2</sub> electrode.....	22
Figure 2.8 Activation energy comparison curve of $\alpha$ -MnO <sub>2</sub> electrode and CMO electrode. [9] ..	22
Figure 2.9 The charge transfer resistance of uncoated ZVO and .....	24
Figure 2.10 The Nyquist plots of the MnO <sub>2</sub> electrode and the MnO <sub>2</sub> @V <sub>2</sub> O <sub>5</sub> electrodes after cycles. (The electrical equivalent circuit for fitting EIS spectra is shown in the inset). [1] .....	25
Figure 2.11 SEM images for electrode before cycles; (a) MnO <sub>2</sub> , (b) MnO <sub>2</sub> @V <sub>2</sub> O <sub>5</sub> .....	26
Figure 2.12 Galvanostatic charge/discharge profiles and cycling performance of bare Zn  MnO <sub>2</sub> cell and SnO <sub>2</sub> @Zn  MnO <sub>2</sub> cell. [13].....	29
Figure 2.13 Relative of cyclic Voltammetry (CV) curve. [16].....	30
Figure 2.14 Example cyclic voltammetry. [16] .....	31
Figure 2.15 Current Diagram – Electric potential difference supplied from the initial (E <sub>initial</sub> ) to the final (E <sub>final</sub> ). [16] .....	32
16Figure 3.1 The components of a CR2025 battery test cell.....	35

17	Figure 3.2 The components of a pouch cell battery.....	36
18	Figure 3.3 Methodology of this research. ....	40
19	Figure 4.1 XRD patterns of the $\alpha$ -MnO <sub>2</sub> nanoparticle.....	42
20	Figure 4.2 XRD patterns of the $\alpha$ -MnO <sub>2</sub> @SnO <sub>2</sub> nanoparticle. ....	43
21	Figure 4.3 EDX mapping of MnO <sub>2</sub> @SnO <sub>2</sub> electrode. ....	44
22	Figure 4.4 FE-SEM images of (a) MnO <sub>2</sub> nanoparticle (high magnification, x50000), (b) MnO <sub>2</sub> electrode (high magnification, x50000) and (c-f) MnO <sub>2</sub> @SnO <sub>2</sub> nanoparticle (high magnification, x50000).....	44
23	Figure 4.5 Cycle performance of MnO <sub>2</sub> , 0.1MS, 0.2MS, 0.3MS and 0.4MS electrodes at current rate 100 mA g <sup>-1</sup> . ....	46
24	Figure 4.6 Rate capability as a function of the current rate (100, 200, 300 and 400 mA g <sup>-1</sup> ) of MnO <sub>2</sub> , 0.1MS, 0.2MS, 0.3MS and 0.4MS electrodes.....	46
25	Figure 4.7 Cyclic voltammetry (CV) curves of (a) MnO <sub>2</sub> , (b) 0.1MS, (c) 0.2MS, (d) 0.3MS and (e) 0.4MS electrodes at scan rate of 0.1 mV s <sup>-1</sup> .....	48
26	Figure 4.8 Nyquist plots of the positive electrode with (a) MnO <sub>2</sub> , (b) 0.1MS, (c) 0.2MS, (d) 0.3MS and (e) 0.4MS electrodes of fresh batteries and after 100 cycles (f) Nyquist plot comparing of after cycling at each electrode. ....	52
27	Figure 4.9 Bode plots of the positive electrode with with (a, b) MnO <sub>2</sub> , (c, d) 0.1MS, (e, f) 0.2MS, (g, h) 0.3MS and (i, j) 0.4MS electrodes. ....	53
28	Figure 4.10 FE-SEM image of positive electrode processed with MnO <sub>2</sub> , 0.1MS, 0.2MS, 0.3MS and 0.4MS electrodes (a, b, c, d, e) before the cycling test and (f, g, h, i, j) after 100 cycles. ....	54
29	Figure 4.11 (a) Pouch cell of the Zinc-MnO <sub>2</sub> and Zinc-MnO <sub>2</sub> @SnO <sub>2</sub> (0.3MS) batteries with positive electrode processed, (b) Electrolytes solution from pouch cell after charge/discharge 20, 40, 60, 80 and 100 cycles,.....	55
30	Figure 4.12 ICP results after different numbers of cycles. ....	56

# CHAPTER 1

## INTRODUCTION

### 1.1 General Introduction

According to current situation the rate of technological advancement is increasing all the time. As a result, researchers are looking at power conversion for safe, cost-effective, and long-lasting large-scale energy storage [1], as well as the portable electronics and automotive industries. Electric motor lithium-ion batteries have been around for a long time. Lithium-ion batteries, on the other hand, suffer issues such as lithium shortages, their highly flammable, toxic, and moisture-sensitive electrolytes hinder their application scene to power the future wearable. There have also been reports of explosions as a result of the massive use of lithium-ion batteries. Therefore, it is imperative to immediately examine the alternative material or battery type thoroughly.

For larger batteries, the rechargeable waterproof ZIB is a viable development alternative. Because of the variety of electrode materials, it is both ecologically beneficial and secure. In addition, the water-based ZIB is presented. This is because it uses an environmentally acceptable aqueous electrolyte with a better ionic conductivity than organic electrolytes and can give more storage capacity with divalent charge transport.

Zinc is frequently utilized as an anode for high energy density aqueous ZIBs because it has excellent gravimetric and volumetric capabilities ( $820 \text{ mAh g}^{-1}$  and  $5855 \text{ mAh cm}^{-3}$ ). Despite the numerous benefits of aqueous ZIBs, finding acceptable cathode materials presents a number of challenges. Manganese-based materials, vanadium-based materials, prussian blue analogs, and polyanionic compounds are the most common cathode materials in aqueous ZIBs. Among all the cathode materials described in the aqueous ZIB manganese oxide ( $\text{MnO}_2$ ) gave a better effect than its Prussian blue analog and has higher working potential than vanadium oxide. This makes manganese oxide the most promising cathode material. Due to the large number of materials, low

cost, good specific capacity and less toxic which is a good feature of manganese oxide and is suitable for use as a cathode for zinc ion aqueous batteries [2].

Despite significant advances in electrochemical performance, these materials suffer from large volume variation, poor electrical, ionic conductivities, the electrode rate performance, and cycling stability are affected by irreversible disintegration during cycling. Manganese oxide has a known problem in which battery capacity will fade quickly. Previous studies have discovered the development of inactive byproducts on the manganese-based cathode surface during the discharge process as a result of the direct contact between the electrode and the electrolyte. Affected by  $\text{OH}^-$  and  $\text{ZnSO}_4$  interaction during proton insertion, the formation of a by-product  $\text{ZnSO}_4(\text{OH})_6 \cdot x\text{H}_2\text{O}$  (ZHS) has occurred [3]. Unfortunately, the formation of by-products ZHS on the surface of the electrode, it disrupts the electrochemical reaction and increases the internal resistance during battery operation, resulting in cathode surface covering and reduction of electrochemical action surface area and impeding electron flow.

In order to solve and improve manganese oxide properties to make them more suitable for use as a cathode in zinc ion battery systems, metal oxide layer coatings have been reported to significantly improve electrochemical performance. As a result, the battery can be used for longer period of time. Another major disadvantage of manganese oxide is its low electrical conductivity. This will hinder the overall performance of the battery. Combining  $\text{MnO}_2$  with highly conductive materials would be a viable solution to this problem. A very simple strategy to overcome this disadvantage consists of modifying the surface with a protective coating. It acts as a protective layer against direct contact between the electrode and electrolyte such as  $\text{Al}_2\text{O}_3$ ,  $\text{TiO}_2$ ,  $\text{ZnO}$ ,  $\text{ZrO}_2$  or  $\text{SiO}_2$ . It can be successfully used to protect host material particles.

Tin oxide ( $\text{SnO}_2$ ) is widely used in the various applications, such as gas sensors, transparent electrodes and solar cells. Such versatile usages are owing to its useful characteristics, for instance, wide band gap energy ( $\sim 3.62$  eV) and high optical transmittance ( $\sim 90\%$ ) and good electrical conductivity ( $0.1\text{-}89$   $\text{S}\cdot\text{cm}^{-1}$ ) [4]. Importantly,  $\text{SnO}_2$  also has higher electrical conductivity than  $\text{TiO}_2$  and  $\text{Al}_2\text{O}_3$ , which are often used as solid electrolyte interfaces (SEI).

However,  $\text{TiO}_2$  and  $\text{Al}_2\text{O}_3$  layers are not suitable for electrically coated layers due to its insulating nature, which reduces electrical conductivity. Therefore, the use of  $\text{SnO}_2$  with good electrical conductivity (0.1- 89 S/cm) to promote and improve  $\text{MnO}_2$  that has disadvantages in electrical conductivity ( $10^{-8} \text{ S}\cdot\text{cm}^{-1}$  at room temperature) and uses the  $\text{SnO}_2$  layer as a solid electrolyte interfaces (SEI) layer. Therefore, it is an interesting approach to develop cathode materials for use in zinc-ion battery systems for long-term use. In addition,  $\text{SnO}_2$  thin film synthesis is actively pursued by scientists and researchers.  $\text{SnO}_2$  thin films are fabricated by various deposition methods such as spray pyrolysis, sol-gel process, thermal plasma deposition, pulsed-laser deposition, electrodeposition, wet-chemical and atomic layer deposition. Among those, the wet-chemical collection methods is the simplest and less expensive than others.

In this work, we synthesized the  $\text{MnO}_2$ -coated  $\text{SnO}_2$  particles by a wet-chemical method to reduce cathode solubility during cycling due to direct contact between the electrode and the electrolyte. This reduces the formation of insulating products (ZHS) at the interface between the electrode/electrolyte on the  $\text{MnO}_2$  cathode [5].

## 1.2 Objective of the research

1.2.1 Find materials used for  $\text{MnO}_2$  cathode coating to improve the surface between the electrode and electrolyte and developed into an SEI layer for the electrode.

1.2.2 Improve the surface of the electrode to reduce the dissolution of  $\text{Mn}^{2+}$  ion and formation of side reaction (ZHS) on manganese dioxide cathode.

1.2.3 Develop  $\text{MnO}_2$  cathode material to high capacity, capable of maintaining battery capacity and can be used for a long time.

### 1.3 Scope of the research

#### 1.3.1 The synthesized of $\alpha$ -MnO<sub>2</sub>

- The pristine  $\alpha$ -MnO<sub>2</sub> nanoparticles were synthesized by a wet-chemical method and annealed at 450 °C for 5h.
- The crystal structure of synthesized samples was examined by X-ray diffraction (XRD) technique.

#### 1.3.2 The synthesized of $\alpha$ -MnO<sub>2</sub>@SnO<sub>2</sub> particles

- The  $\alpha$ -MnO<sub>2</sub>@SnO<sub>2</sub> particles were created using a wet-chemical method and were calcined at 400° C for 1 h in an ambient atmosphere to obtain Sn coated MnO<sub>2</sub>, studied at different SnO<sub>2</sub> ratios i.e., 0.1MS, 0.2MS, 0.3MS and 0.4MS.
- The crystal structure of synthesized samples was examined by X-ray diffraction (XRD) technique.
- The morphology of samples was analyzed using a field emission scanning electron microscopy (FE-SEM) and Energy dispersive X-ray (EDX).

#### 1.3.3 Preparation of $\alpha$ -MnO<sub>2</sub> and $\alpha$ -MnO<sub>2</sub>@SnO<sub>2</sub> electrode

- To fabricate the working electrode, a slurry consisting of 80 wt.%  $\alpha$ -MnO<sub>2</sub> or  $\alpha$ -MnO<sub>2</sub>@SnO<sub>2</sub> (0.1MS, 0.2MS, 0.3MS and 0.4MS), 10 wt.% carbon black, and 10 wt.% binder was prepared.
- Polyvinylidene Fluoride binder (PVDF) in N-Methyl-2-Pyrrolidone (NMP) solvent is binder for electrode.
- Battery Performance, which is elucidated using Galvanostatic charge-discharge cycling of the battery was measured using a battery analyzer, cyclic voltammetry (CV), and electrochemical impedance spectroscopies (EIS).

#### 1.3.4 Study of electrode properties.

- The solubility of the electrodes was studied with the ICP test.

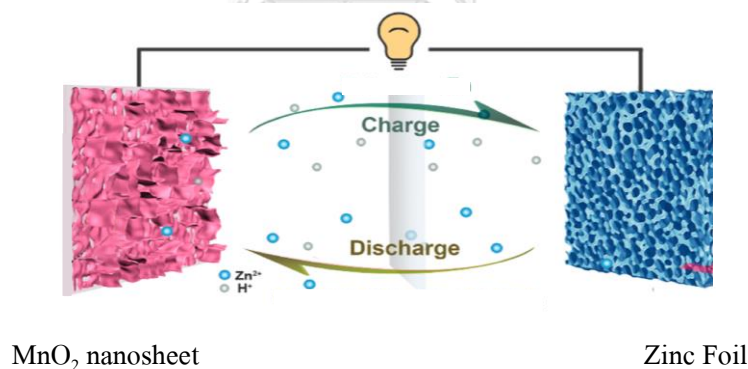
## CHAPTER 2

### THEORY AND LITERATURE REVIEWS

#### 2.1 Mechanistic study of Zinc-ion battery

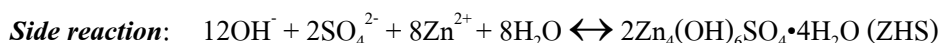
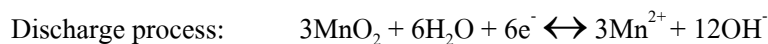
The battery configuration in this study, which is composed of the  $\text{MnO}_2$  cathode, zinc anode, and  $\text{ZnSO}_4$  aqueous electrolyte is shown. During discharging, anodic zinc is dissolved in the form of  $\text{Zn}^{2+}$  ions into an aqueous electrolyte, containing  $\text{Zn}^{2+}$  ions and rapidly solvate in the form of solvated  $\text{Zn}^{2+}$  ion. Then, they diffuse and pass through the separator to the  $\text{MnO}_2$  cathode. The solvated  $\text{Zn}^{2+}$  ions are de-solvated in the form of  $\text{Zn}^{2+}$  ions and intercalate into  $\text{MnO}_2$  structure as illustrated by the inset of figure 2.1.

Further, an electron current starts to flow in the electrical loop from the electrical conduction of graphite. These three processes can be reversed by (1) the de-intercalation of  $\text{Zn}^{2+}$  ions from  $\text{MnO}_2$  cathode; then (2) solvated species are formed and lastly (3)  $\text{Zn}^{2+}$  ions are reduced to Zn and deposited back on the zinc anode, respectively.



**Figure 2.1** Schematic representation of electrolytic process and structure change process of the aqueous rechargeable Zn/ $\text{MnO}_2$  battery in  $2\text{M ZnSO}_4 + 0.5\text{M MnSO}_4$  electrolyte.

To understand the mechanism of charge storage in aqueous zinc-ion batteries. Electrode reaction in charge/discharge process and the electrochemical reaction of  $\text{ZnSO}_4(\text{OH})_6 \cdot x\text{H}_2\text{O}$  was thoroughly investigated, as shown in the equation below [6, 7].

***First cycle***

During the first cycle release process, the  $\text{MnO}_2$  host material reacts with  $\text{H}_2\text{O}$  molecules to form  $\text{Mn}^{2+}$  and  $\text{OH}^-$  products. The electrolyte for the zinc ion battery system is  $\text{ZnSO}_4$ , and it reacts immediately with the developing  $\text{OH}^-$ . Thus, the formation of ZHS (cathode surface-adhesive insulators), reduces the amount of  $\text{H}_2\text{O}$  around the  $\text{MnO}_2$  molecule, contributing to battery performance. As a result, the subsequent dissolution of  $\text{MnO}_2$  is slower in the absence of less active  $\text{H}_2\text{O}$ . The latest generation ZHS combines with  $\text{Mn}^{2+}$  to form birnessite- $\text{MnO}_2$  and decrease the  $\text{Mn}^{2+}$  content and the pH value. In subsequent cycles, the same dissolution-deposition mechanism happens. However, this time the host material is birnessite- $\text{MnO}_2$  rather than pristine  $\text{MnO}_2$ .

#### 2.1.1 Side reaction: The formation of $\text{ZnSO}_4(\text{OH})_6 \cdot x\text{H}_2\text{O}$ (ZHS)

**Xun Guo et al (2020) [7]** was explored the reaction kinetics of ZHS in detail following the ex-situ galvanostatic discharge/charge experiments. After acid pickling for 20 minutes, it is obvious that ZHS may be rinsed with acetate buffer, and a substantial amount of  $\text{MnO}_2$  was exposed without ZHS masking. This section shows that even the formation of ZHS can decay during the charging process. However, there were some that remained. As a result, a ZHS insulator forms on the electrode surface, explaining the decreased capacity compared to theoretical specific capacity. Because of the created ZHS, a substantial amount of active  $\text{H}_2\text{O}$  near  $\text{MnO}_2$  will be removed, as seen in Figure 2.2. In addition, because ZHS covers the entire cathode surface,  $\text{H}_2\text{O}$  is prevented from touching the  $\text{MnO}_2$  cathode material. The absence of active  $\text{H}_2\text{O}$  for use in the next cycle effectively inhibits the subsequent dissolution process of  $\text{MnO}_2$ . This results in difficulty in the ability to achieve specific theoretical abilities.

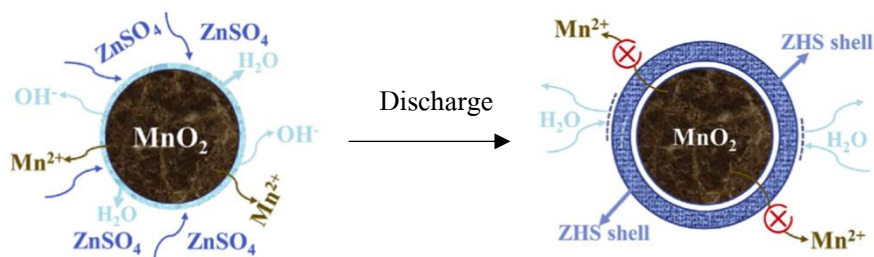


**Figure 2.2** The role of ZHS in the discharge process. [5]

Hence, different acid pickling treatment times were used to achieve varying levels of ZHS coverage. The discharge capacity increased from  $19.6 \text{ mAh g}^{-1}$  (2 min) to  $115.8 \text{ mAh g}^{-1}$  (8 min) as the acid treatment time increased. As shown in Figure 2.3, it is evident from the results of this test that the formation of ZHS plays an important role in the reaction kinetics and electrode capacitance. During the release process which results in the subsequent dissolution of  $\text{MnO}_2$ .

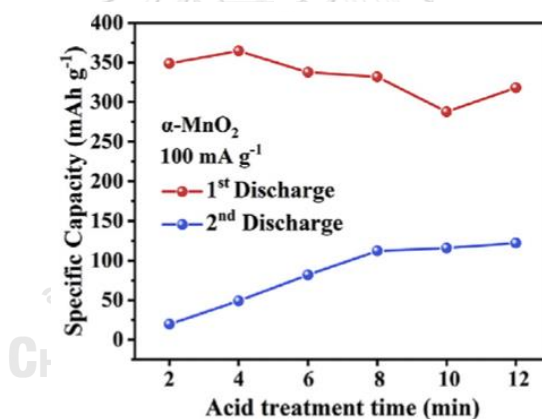


**Figure 2.3** The capacitance of  $\text{MnO}_2$  electrodes in  $2\text{M ZnSO}_4$  electrolytes after washing in acetate buffer for different times to eliminate ZHS formation. [5]

Thus, reducing the formation of ZHS to form on the surface of the electrode, it will be beneficial to the battery performance. One strategy is to modify textures, which can create a good interface with the electrolyte instead of direct contact of the electrode. Here we will discuss the construction of a solid electrolyte interphase (SEI) layer for the electrode in aqueous Zinc-ion battery (ZIBs) systems.

### 2.1.2 Dissolution of manganese-based oxide

Because of the typically employed (slightly) acidic electrolytes, metal oxide cathodes are prone to metal dissolution during battery operation. The technique for monitoring manganese-based oxide dissolution and structural evolution has been extensively studied. Surface coating, electrolyte optimization, and composition tweaking are all suggested as effective remedies to this problem [6].

Ce Qiu et al (2020) [8] monitored the dissolution of manganese-based oxide and the structural evolution by analyzing the  $\text{Mn}^{2+}$  ion concentration in electrolyte solution and electrochemical performances through inductively coupled plasma (ICP) and CV techniques. They discovered that mixing  $\text{MnSO}_4$  into a moderate  $\text{ZnSO}_4$  aqueous electrolyte changes the dissolving equilibrium of  $\text{Mn}^{2+}$  from the  $\text{MnO}_2$  electrodes, suppresses continuous  $\text{Mn}^{2+}$  dissolution, and improves capacity decay significantly. Furthermore, the addition of  $\text{MnSO}_4$  to the electrolyte had no effect on the redox processes in the  $\text{MnO}_2$  electrode. After 800 cycles, this Zn/ $\text{MnO}_2$  battery with 0.5M  $\text{MnSO}_4$  in the electrolyte may achieve the highest specific capacity of roughly 200  $\text{mAh g}^{-1}$ .

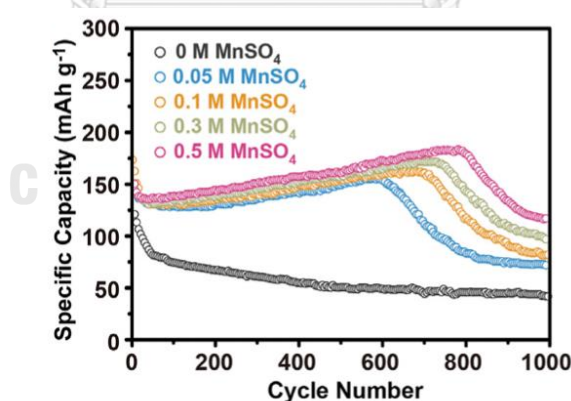


**Figure 2.4** Cycle performances of the Zn/ $\delta\text{-MnO}_2$  cells using different electrolytes for 1000 cycles at a current density of 200  $\text{mA g}^{-1}$ . [7]

## 2.2 Solid electrolyte interphase (SEI)

In a lithium-ion battery, the solid electrolyte interface (SEI) is critical. SEI films, on the other hand, can be placed in a solvent and remain stable. It can also be utilized to prevent things from dissolving or the creation of co-solvent molecules. Both things can help protect the cathode material and increase the efficiency of the cycle and the life of the cathode. On the other hand, SEI allows lithium ions to pass through but prevents electrons from passing through. Thus, the charge/discharge cycle of lithium-ion batteries can be maintained better, and the battery life is extended [9].

However, the solid electrolyte interface (SEI) coating on the cathode surface is rarely discussed. Cathode material dissolving is prevalent in aqueous ZIBs, resulting in significant performance degradation. As a result, understanding the structure of the cathode side SEI protective coating in water systems is critical. The goal is to create a long-lasting liquid battery and reduce the solubility problem of the cathode material.

### 2.2.1 Naturally Solid electrolyte interface (SEI)

**Shan Guo et al.,(2019)** [9] studied the  $\text{Ca}_2\text{MnO}_4$  (CMO) cathode, which demonstrated the presence of solid electrolyte interface (SEI) layer  $\text{CaSO}_4 \cdot 2\text{H}_2\text{O}$  (CS). It is generated on the surface of CMO during in situ charging process for an aqueous zinc-ion battery. The presence of the SEI coating has a significant impact on the cathode's structural integrity as it approaches disintegration.

The diffusion coefficient of CMO in the charging process was close to that of standard  $\text{MnO}_2$  utilizing the galvanostatic intermittent titration technique in the electrochemical performance test of  $\text{CMO@CS}$  as depicted in Figure 2.5. This is owing to CMO excellent structural properties (the presence of the SEI layer on the cathode side). Furthermore, during the discharge process, the diffusion coefficient of CMO was much higher than that of  $\text{MnO}_2$  in the later stages of discharge. Because of the existence of the SEI layer, CMO outperforms  $\text{MnO}_2$  (Shadow region in Figure 2.5).

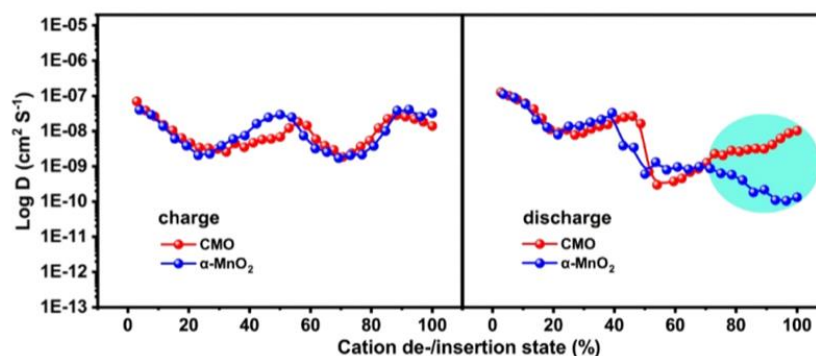


**Figure 2.5** Diffusion coefficient contrast curve of CMO and  $\alpha\text{-MnO}_2$ . [9]

The degradation of  $\text{MnO}_2$  capacitance occurs primarily near the end of the discharge phase. The critical CMO remained more stable at the end of the discharge phase, as illustrated in Figure 2.6 by the  $100 \text{ mA g}^{-1}$  AC discharge curve of  $\text{MnO}_2$  and the CMO still exhibits greater stability, and has a higher capacitance than the  $\text{MnO}_2$  electrode, which is consistent with the diffusion coefficient values shown in Figure 2.5.

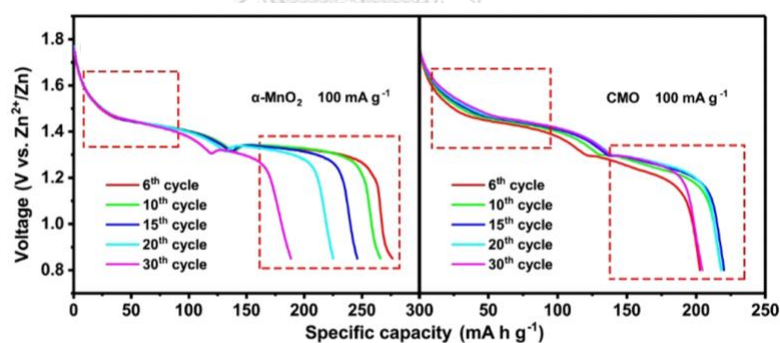


**Figure 2.6** The galvanostatic discharge comparison curve in  $100 \text{ mA g}^{-1}$  of  $\alpha\text{-MnO}_2$  electrode and CMO electrode. [9]

Inductively coupled plasma optical emission spectrometry (ICP-OES) is used to assess the manganese ion solubility in the electrolyte, as shown in Figure 2.7. The manganese solubility rate for CMO in  $\text{ZnSO}_4$  (ZS) electrolyte is substantially lower than that for  $\text{MnO}_2$  in  $\text{ZnSO}_4$  electrolyte and CMO in  $\text{Zn}(\text{CH}_3\text{COO})_2$  (ZA) electrolyte, indicating that the rate of manganese dissolving into the electrolyte on the CMO electrode is optimal. The surface-coated  $\text{CaSO}_4 \cdot 2\text{H}_2\text{O}$

(CS) layer (SEI) has been shown to prevent manganese solubility in the water system, improving battery stability and lifespan.

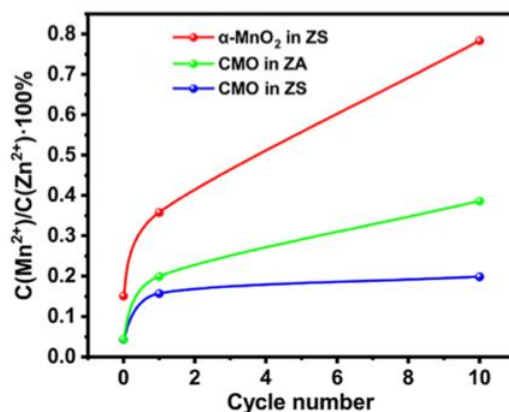


**Figure 2.7** Comparison of manganese dissolution rate of  $\alpha\text{-MnO}_2$  electrode and CMO electrode in different electrolytes. [9]

A graph comparing the activation energy of  $\text{MnO}_2$  and CMO electrodes at the fully charged state is given in Figure 2.8. It was discovered that the CMO electrode had a lower interface activation energy than the  $\text{MnO}_2$  electrode based on the Electrochemical Impedance Spectroscopy (EIS) test. This means that the charge transfer resistance is low and cause easy charge transfer. As a result, producing a  $\text{CaSO}_4 \cdot 2\text{H}_2\text{O}$  (CS) layer (SEI) coating can help improve the interface while also enabling the electrode reaction.

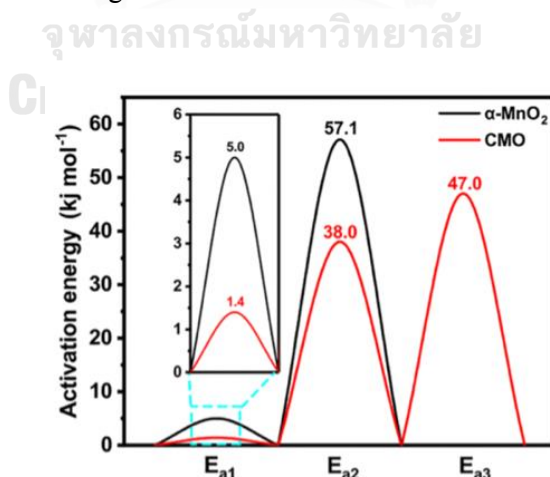


**Figure 2.8** Activation energy comparison curve of  $\alpha\text{-MnO}_2$  electrode and CMO electrode. [9]

The SEI film coating on the CMO electrode prevents manganese ions from dissolving and protects the CMO cathode. In the meantime, this in situ generated interface layer is useful for lowering impedance, improving the interface, and lowering activation energy. As a result, rate performance and cycle stability are greatly improved. These sections emphasize the benefits of having a stable layer of SEI film placed on the electrode surface.

### 2.3 The Solid electrolyte interphase (SEI) layer in zinc ion batteries.

It has been proven that covering electrode materials with a coating of metal oxide that is stable improves their electrochemical performance significantly. Because of the abundant materials and low cost, metal oxide coating modification has been widely used in the development of electrodes for lithium-ion batteries. On the other hand, metal oxide coating modification on the cathode for aqueous ZIBs is rarely reported.

In a zinc-ion battery system, **Jing Guo et al.,(2019)** [3] investigated the cathode material vanadium oxide. To improve the solubility of vanadium in the electrolyte and the formation of a side reaction, ultrathin  $\text{HfO}_2$  sheet was created using atomic layer deposition (ALD) as an artificial solid electrolyte interphase (SEI). The resulted of the  $\text{HfO}_2$ -coated ZVO electrode and the uncoated ZVO electrode were compared in a test. The results of a galvanostatic charge/discharge test. The  $\text{HfO}_2$ -coated ZVO electrode was able to maintain a decent capacity of 90% after 100 cycles of use, which was stated as a battery capacity of  $227 \text{ mAh g}^{-1}$ . After the same number of cycles of application, the uncoated ZVO electrode can only maintain capacitance of 45%, which is stated as the anticipated battery capacity of  $100 \text{ mAh g}^{-1}$ . This signifies a considerable capacity loss.

The amount of electrode dissolution into the electrolyte during cycling was determined using ICP-OES measurements. After being utilized for several time, The concentration of vanadium in pure ZVO dissolved in the electrolyte rose as the turnover increased. This shows that the active substance and the mildly acidic electrolyte are in direct contact. As a result, vanadium corrosion is becoming more prevalent. On the other hand, the  $\text{HfO}_2$ -coated ZVO cathode shows

much less dissolution of vanadium into the electrolyte, which corresponds to superior performance.

The reaction between ZVO and electrolyte, which leads to an insulating layer produced on the cathode surface, is responsible for the reported reversible creation of ZHS. It is worth noting that this byproduct has a substantial impact on the electrochemical reaction during the discharge process, as evidenced by the ex-situ EIS measurement as shown in Figure 2.9. At different charge/discharge steps, the charge transfer resistance ( $R_{ct}$ ) of the two samples, the  $R_{ct}$  of the ZVO electrode increased significantly during the discharging phase, then decreased to approximately its original value during the charging phase. This is due to the formation of some byproducts which insulate the electrode surfaces. This results in increased internal resistance. This is because the increased insulating layer impedes electron transport. When compared to the  $HfO_2$ -coated ZVO electrode, the charge transfer resistance ( $R_{ct}$ ) gradually changes, and no overestimation appears. The  $HfO_2$  layer, which acts as an artificial passive layer which prevents the synthesis  $ZnSO_4(OH)_6 \cdot xH_2O$  was achieved, resulting in no insulating formation on the electrode surface.

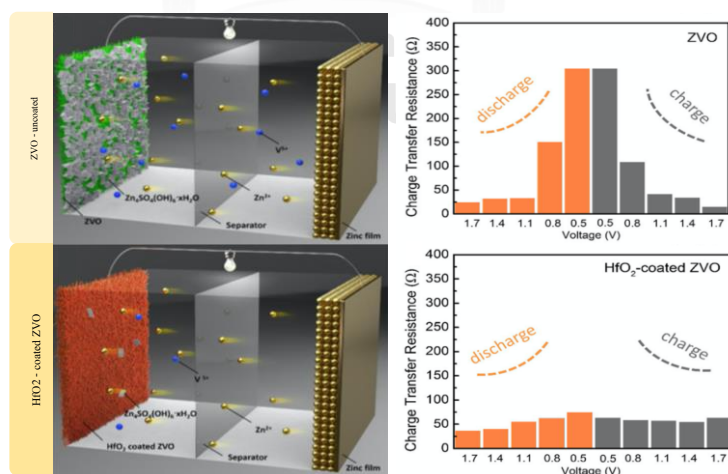


**Figure 2.9** The charge transfer resistance of uncoated ZVO and  $HfO_2$ -coated ZVO during the charge and discharge process. [3]

**Hongjing Shang et al.,(2020)** [1] investigated the cathode of vanadium pentoxide  $V_2O_5$ -coated  $MnO_2$ . This study highlights the possibility of Zn-ion conductor oxide coating as a strategy for improving  $MnO_2$  electrochemical performance in aqueous ZIBs.

Electrochemical results were compared to  $MnO_2$  electrodes using  $MnO_2@V_2O_5$  electrodes in the study. At the same current density, the  $MnO_2@V_2O_5$  electrode galvanostatic charge/discharge profile gives a more stable and greater capacitance than the  $MnO_2$  electrode. Meanwhile, the  $MnO_2@V_2O_5$  electrode demonstrates an activation phenomena at  $0.1\text{ A g}^{-1}$ , with a progressive rise in capacity to  $381.4\text{ mAh g}^{-1}$  after 47 cycles and a capacity retention of 98.7% after 80 cycles, whereas the  $MnO_2$  electrode shows evident attenuation.

The Nyquist plot of the  $MnO_2@V_2O_5$  electrode as shown in Figure 2.10 is significantly smaller than that of the  $MnO_2$  electrode, showing that the  $MnO_2@V_2O_5$  electrode has a lower  $R_{ct}$  resistance. As a result, it has been discovered that altering the surface of the  $V_2O_5$  coating can improve charge transfer at the electrode/electrolyte contact, which is good for electrochemical performance.

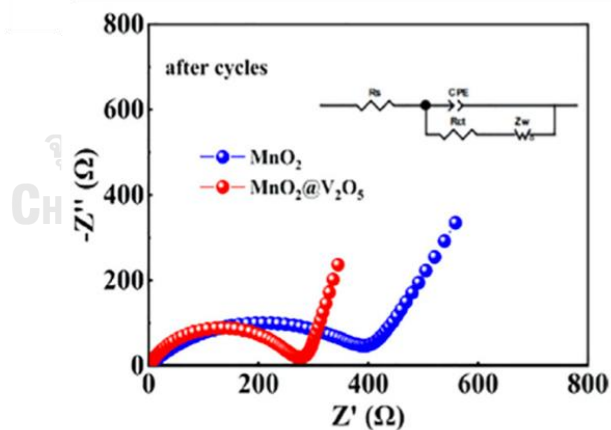


**Figure 2.10** The Nyquist plots of the  $MnO_2$  electrode and the  $MnO_2@V_2O_5$  electrodes after cycles. (The electrical equivalent circuit for fitting EIS spectra is shown in the inset). [1]

The surface of the electrode morphology was studied using SEM images, the  $\text{MnO}_2$  electrode surface shape before cycling is made up of spherical particles. As illustrated in Figure 2.11c, the  $\text{MnO}_2$  electrode has evident cracks and holes after cycling, which are induced by significant volume fluctuations and  $\text{MnO}_2$  dissolution during charge/discharge. In comparison, clean microspheres can also be seen in the  $\text{MnO}_2@V_2O_5$  electrode, as shown in Figure 2.11b. Despite a few cracks on the  $\text{MnO}_2@V_2O_5$  electrode surface, the microsphere survives, demonstrating the structural durability of  $V_2O_5$  and its contribution to the preservation of the spherical  $\text{MnO}_2$  shape, as shown in Figure 2.11d. On the other hand, reduce  $\text{MnO}_2$  volume expansion and inhibit electrode powdering, resulting in greatly improved  $\text{MnO}_2$  cycle stability during charging and discharging.

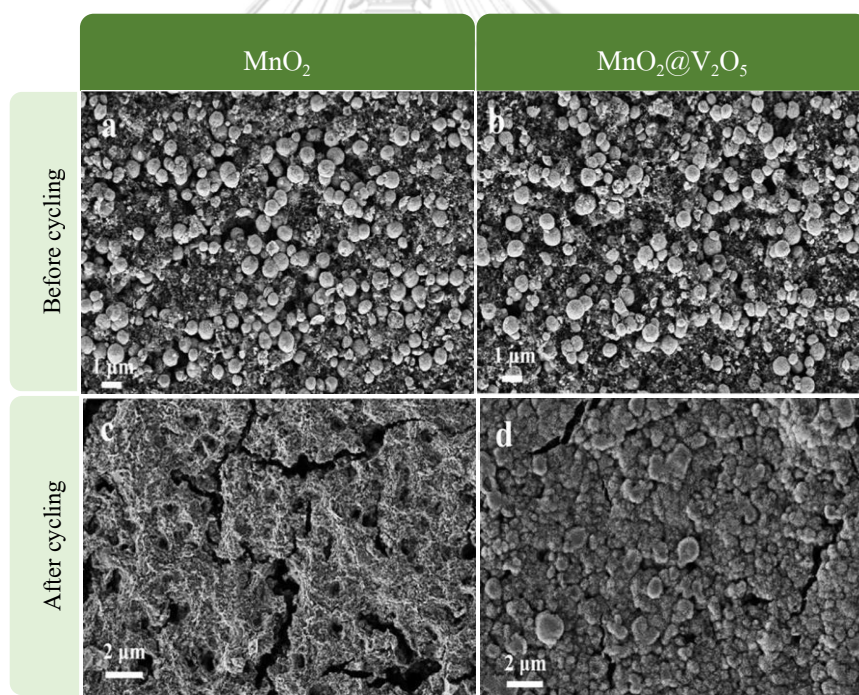


**Figure 2.11** SEM images for electrode before cycles; (a)  $\text{MnO}_2$ , (b)  $\text{MnO}_2@V_2O_5$   
And SEM images for electrode after cycles; (c)  $\text{MnO}_2$ , (d)  $\text{MnO}_2@V_2O_5$  [1]

**Lei Gou et al., (2019)** [10] studied a new coating approach involving  $\text{In}_2\text{O}_3$  to improve the intrinsic low conductivity of cathode materials. They used a simple and mild hydrothermal technique to make  $\text{In}_2\text{O}_3$  coated  $\text{MnO}_2$ .

Electrochemical tests of charge/discharge capabilities after the  $\text{In}_2\text{O}_3$  coating reveal that  $\text{MnO}_2@ \text{In}_2\text{O}_3$  has a potential difference of 0.27 V, which is lower than  $\text{MnO}_2$  is 0.34 V. The  $\text{MnO}_2@ \text{In}_2\text{O}_3$  electrode exhibits a lower polarization and better electrochemical reaction kinetics due to the increased electrical conductivity created by the  $\text{In}_2\text{O}_3$  coating. At a current density of 100  $\text{mA g}^{-1}$ , the cycling performance of  $\text{MnO}_2$  and  $\text{MnO}_2@ \text{In}_2\text{O}_3$  electrodes is compared. The charge/discharge at a current density of 100  $\text{mA g}^{-1}$ . To compare the cycling efficiency of the  $\text{MnO}_2$  and  $\text{MnO}_2@ \text{In}_2\text{O}_3$  electrodes, it was found that the capacitance of the  $\text{MnO}_2$  electrodes decreased rapidly after 100 cycles of use. Starting capacity 200  $\text{mAh g}^{-1}$  can maintain only 78% capacity. With the same number of cycles,  $\text{MnO}_2@ \text{In}_2\text{O}_3$  electrodes can improve battery performance and showing capacities up to 425  $\text{mAh g}^{-1}$ . These findings suggest that  $\text{In}_2\text{O}_3$  coating can greatly improve battery performance, and  $\text{In}_2\text{O}_3$  plays a role in preserving better capacity. The  $R_{ct}$  resistance of  $\text{MnO}_2@ \text{In}_2\text{O}_3$  electrodes is lower, according to electrochemical impedance spectroscopies (EIS). As a result, the surface modification of the  $\text{MnO}_2$  cathode by  $\text{In}_2\text{O}_3$  coating allows for significantly better charge transfer at the electrode/electrolyte interface and lowers overall battery internal resistance, resulting in increased electrochemical performance.

In summary, the data show that  $\text{OH}^-$  interacts with  $\text{ZnSO}_4$  during the discharge process, forming a significant amount of  $\text{ZnSO}_4(\text{OH})_6 \cdot x\text{H}_2\text{O}$  (ZHS) on the electrode surface. The formation of by-products ZHS forms an insulating layer over the electrode surface, thereby increasing the internal resistance of the entire battery and inhibiting the reaction by reducing the electrochemical active area during cycling. It negatively affects the output power and endurance of cycling, decreasing the overall performance of the battery. The electrode and electrolyte can be separated directly using an ultrathin SEI layer created using various ways. On the one hand, due to the various features of the interface, the development of the byproduct (ZHS) could be successfully prevented, resulting in a larger capacity. On the one hand, due to the differing properties of the interface, the production of a side reaction (ZHS) could be successfully

prevented. This may be due to the resulting SEI layer altering the surface interaction between the electrode and electrolyte, resulting in a greater battery capacity. The SEI layer prevents direct contact between the cathode and the electrolyte. This reduces the dissolution of the active material [11]. At the same time,  $Zn^{2+}$  can easily flow through the interface area. It was shown that the latent layer had no effect on the diffusion kinetics of  $Zn^{2+}$  due to the amorphous nature of the SEI layer [12].

#### 2.4 Tin oxide, $SnO_2$

Tin oxide ( $SnO_2$ ) is an important wide band gap n-type semiconductor and exhibits unique electrical, optical, physical, and chemical properties.  $SnO_2$  has been widely used in various fields, such as photo catalysis, transparent conducting electrodes, gas sensors and lithium/sodium-ion batteries.

The study of metal oxide layer coatings at the anodes in zinc ion batteries revealed that  $TiO_2$  and  $Al_2O_3$  layers are not suitable for electrolytic coatings due to their insulating properties, which reduced their electrical conductivity. It also shows that the  $SnO_2$  layer has a better electrical effect than the  $Al_2O_3$  and  $TiO_2$  coatings.

**Sang Hyuk Gong et al.,(2019)** [13] study the application of an  $SnO_2$  layer on zinc electrodes used as anodes for zinc ion batteries aiming to solve the problem of dendrite growth. The battery performance was greatly improved after the tin oxide layer was applied with the ALD method. Due to the presence of a tin oxide layer, the formation of dendrites can be reduced. It also helps alleviate hydrogen gas evolution. When looking at the performance of a full-cell battery. Comparison between batteries with bare zinc anode and tin oxide coated zinc and manganese dioxide is used as the cathode electrode. It can be seen that the performance of the battery improved with the tin oxide layer is noticeably good. This is because the tin oxide layer is able to suppress the growth of dendrites on the anode. Where the formation of dendrites results in a short circuit, It also helps to alleviate the hydrogen gas evolution, resulting in a battery's overall performance that can be used for a longer period of time.

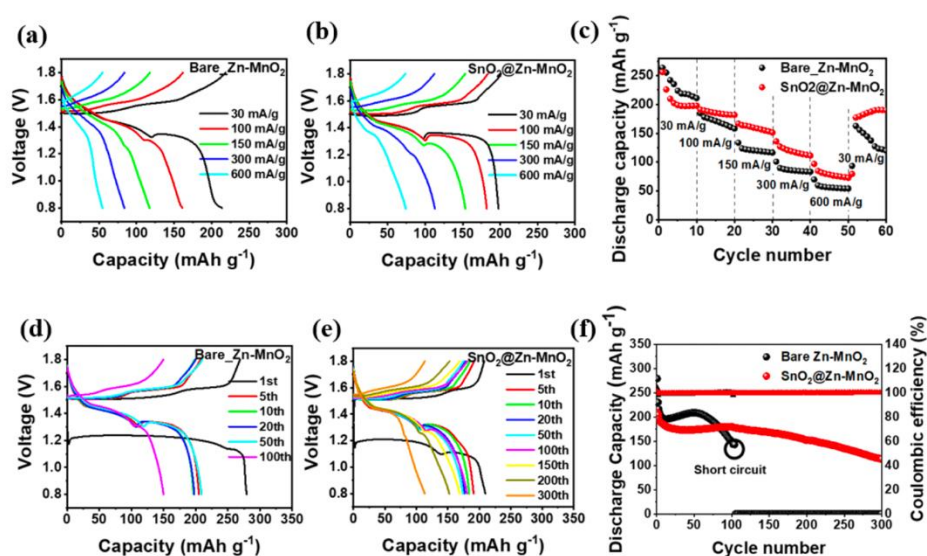


**Figure 2.12** Galvanostatic charge/discharge profiles and cycling performance of bare Zn||MnO<sub>2</sub> cell and SnO<sub>2</sub>@Zn||MnO<sub>2</sub> cell. [13]

From the information presented, it is shown that using SnO<sub>2</sub> as an artificial SEI to passivate the electrode surface improves the performance of aqueous ZIBs substantially [14]. In terms of capacitance and cycling stability, SnO<sub>2</sub> coating of the electrode outperforms the pristine MnO<sub>2</sub> electrode. It has been established that the capacity fading process works [15]. It demonstrates that during the loop process, the fake SEI layer serves two objectives. It functions as a barrier between the electrode and the electrolyte, preventing direct contact, prevents active components from dissolution and forming insulating byproducts in the electrolyte. This method has been shown to function with a variety of cathode materials, demonstrating the universality of our artificial SEI method.

Therefore, in order to improve the irreversible dissolution during cycling and formation of ZnSO<sub>4</sub>(OH)<sub>6</sub>·xH<sub>2</sub>O covering the surface of manganese oxides electrode to be used electrode for aqueous zinc ion battery, the SnO<sub>2</sub> coating with different proportions were studied.

## 2.5 Analytical Techniques

A variety of characterization techniques were used in battery research. These were used not only to characterize the battery cells, but also to determine cell parameters. The power-energy, cycling behavior, charge transfer characteristics change during cycling, and electrode-electrolyte interphase can all be investigated using the techniques listed below.

### 2.5.1 Cyclic Voltammetry (CV)

Cyclic Voltammetry (CV) is a survey of the electrode system in an electrolyte solution. To determine whether the system has a redox reaction between the electrodes and the electrolyte solution or is due to the catalyst properties of the electrodes themselves. By distributing the electric potential difference in a triangle or the electric potential difference oscillates during the use of the electrodes in the electrolyte solution. The potential difference applied to this method is shown in Figure 2.13.

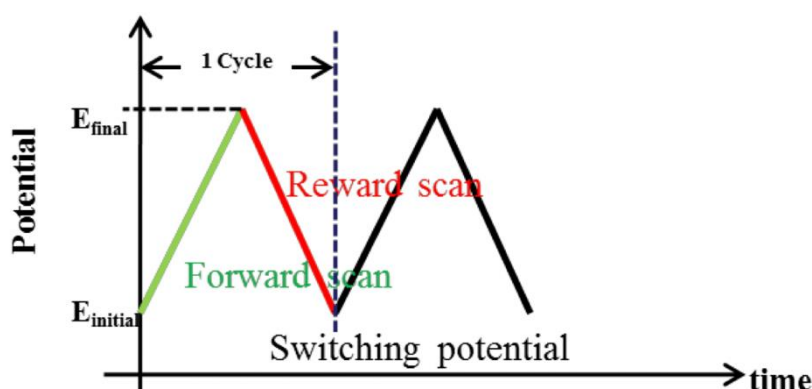


**Figure 2.13** Relative of cyclic Voltammetry (CV) curve. [16]

The measured value is the electric current generated due to the transmission of electrons in and out of the terminals when the potential difference from small to large. The positive current is the anodic current and the negative side is the cathodic current. The anodic current is caused by electrons leaving the electrodes to the ions in the solution and the cathodic current takes place

through electrons in turn diagram between the electric potential difference applied to the measured current value at any potential difference.

The measured current is plotted as a function of the potential in a graph known as a voltammogram. The example voltammogram in Figure 2.14 shows four voltage vertices: E1 (initial potential), E2 (second, switching potential), E3 (third, switching potential), and E4 (final potential). The voltage peaks in the waveform are the anodic ( $E_{pa}$ ) and the cathodic ( $E_{pc}$ ) peak potentials. From the potential sweep, important information about the experiment can be derived and analyzed [16].

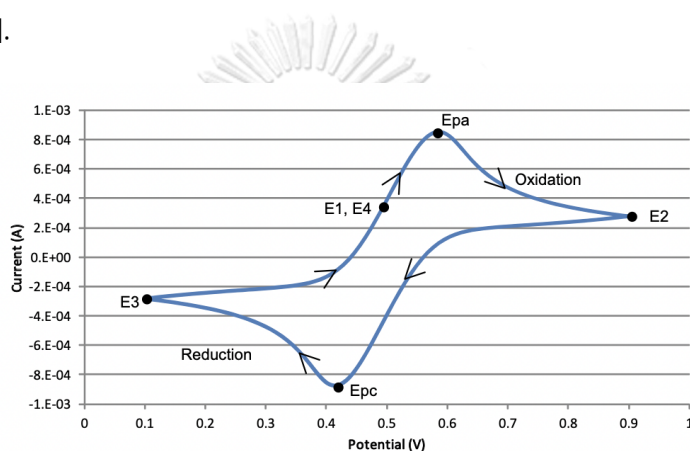


**Figure 2.14** Example cyclic voltammetry. [16]

### 2.5.2 Electrochemical Impedance Spectroscopy (EIS)

Electrochemical impedance spectroscopy (EIS) is a very useful technique for characterization of electrochemical systems which may help to differentiate the influence of physical and a chemical phenomenon at a certain electric potential with just one step of the experiment, they were gathered.

The graph showing the relationship between the real part and the imaginary part of the impedance is called the Nyquist plot as shown in Figure 2.15 and to be able to easily understand it the graph used for display should be equal in size to the physical and imaginary axes to prevent distorting the shape of the graph. The shape of the graph is important in describing the qualitative aspect of the data.

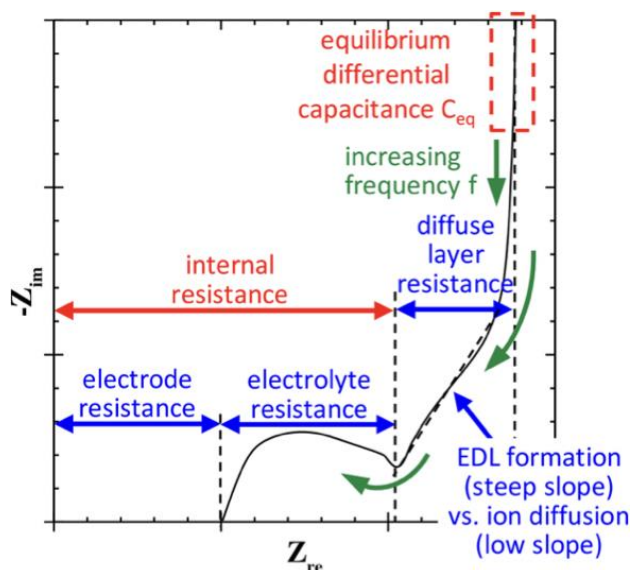


**Figure 2.15** Current Diagram – Electric potential difference supplied from the initial ( $E_{initial}$ ) to the final ( $E_{final}$ ). [16]

The signal obtained from the impedance measurement is the current value as a sinusoidal signal. The current signal represents the physical nature of the interface between the electrodes and the solution.

### 2.5.3 Galvanostatic charge-discharge Test

A standard method for determining battery cell efficiency and energy cycling capability is the galvanostatic charge-discharge test to provide power and charging current to the cell on a regular basis while staying within the rated voltage. The end result is a voltage profile that is time-based. The results can be used to calculate the current density, specific charge/discharge capacitance, and coulombic efficiency. In general, the test current is normalized with the amount of active host material that the electrode has as shown in equation below.

$$\text{Current Density} = \frac{I}{m_{ac}}$$

The total charge is used to calculate the capacity of the positive electrode. When charging or discharging, this is delivered from the positive electrode. This could be obtained by integrating the current with respect to the time between the initial and cut-off states, then normalize this value by the mass of the active material ( $m_{ac}$ ), as shown in equation below.

$$\text{Specific Capacity} = \frac{1}{m_{ac}} \left( \int_{t_0}^{t_f} I dt \right)$$



## CHAPTER 3

### METHODOLOGY

#### 3.1 Materials

Reagent grade chemicals were obtained and used without further purification unless noted otherwise. Potassium permanganate ( $\text{KMnO}_4$ ; AR grade, M.W. 158.034 g/mol), Manganese(II) acetate tetrahydrate ( $\text{Mn}(\text{CH}_3\text{COO})_2 \cdot 4\text{H}_2\text{O}$ ; AR grade, M.W. 245.09 g/mol), Tin(II) chloride dihydrate ( $\text{SnCl}_2 \cdot 2\text{H}_2\text{O}$ ; AR grade, M.W. 225.65 g/mol), Manganese sulfate monohydrate ( $\text{MnSO}_4 \cdot \text{H}_2\text{O}$ ; AR grade, M.W. 169.02 g/mol), Zinc sulfate 7-hydrate ( $\text{ZnSO}_4 \cdot 7\text{H}_2\text{O}$ ; AR grade, M.W. 287.58 g/mol), Supper Carbon (Supper P, Timcal), Polyvinylidene Fluoride (PVDF), N-Methyl-2-Pyrrolidone (NMP), Graphite foil (Thickness: 0.05, 0.1 mm), Glass microfiber paper (GF/A, Whatman: 1.2  $\mu\text{m}$ ), Zn sheet 99.99% (Thickness: 0.1 mm), and blank coin cell CR2025.

#### 3.2 Material Synthesis.

##### 3.2.1 Synthesis of $\alpha\text{-MnO}_2$

The pristine  $\alpha\text{-MnO}_2$  nanoparticles were synthesized by dissolving 150 mmol of  $\text{Mn}(\text{CH}_3\text{COO})_2 \cdot 4\text{H}_2\text{O}$  in 30 mL of deionized (DI) water (denoted: solution A). Then, 100 mmol of  $\text{KMnO}_4$  in 50 mL of deionized (DI) water was added dropwise to solution A. Following the addition of the  $\text{KMnO}_4$  solution and continuous stirring for 5 hours, a dark brown precipitate was obtained. The resulting products were then filtered, washed with distilled water, then ethanol, and dried for 12 hours at  $80^\circ\text{C}$ . Finally, before characterization, the as-prepared sample was ground with an agate mortar and annealed at  $450^\circ\text{C}$  for 5 hours [17].

##### 3.2.2 Synthesis of $\alpha\text{-MnO}_2@\text{SnO}_2$

To make the  $\text{SnO}_2$ -coated samples,  $\text{SnCl}_2 \cdot 2\text{H}_2\text{O}$  was used as a coating agent. In 50 mL of absolute ethanol, 1 g of  $\text{MnO}_2$  was mixed with 0.1, 0.2, 0.3 and 0.4 g of  $\text{SnCl}_2 \cdot 2\text{H}_2\text{O}$  for 3 hours at room temperature. To evaporate the ethanol, more stirring at  $80^\circ\text{C}$  was performed. After completely vaporizing the ethanol, the dried sample was calcined in an atmosphere at

400°C for 1 hour to obtain Sn coated  $\text{MnO}_2$  (hereafter referred to as 0.1MS, 0.2MS, 0.3MS, 0.4MS) [18].

### 3.3 Positive Electrode Fabrication

#### 3.3.1 Coin cell

To fabricate the working electrode, a slurry consisting of 80 wt.%  $\text{MnO}_2$  or  $\text{MnO}_2@\text{SnO}_2$  (0.1MS, 0.2MS, 0.3MS, 0.4MS), 10 wt.% carbon black, and 10 wt.% binder was prepared [19]. Then, using a doctor blade machine, the electrode was then coated with a 25  $\mu\text{m}$  thickness of the mixture on a graphite sheet with a thickness of 0.05 mm. Next, the solvent was then removed by drying it under vacuum. After processing, the electrode was sliced into round disks for the cathode electrode in  $\text{Zn}/\text{MnO}_2$  complete cells (diameters = 15 mm). When fabricating the battery, CR2025 coin cells were used in the battery's construction. A composite  $\text{MnO}_2$  or  $\text{MnO}_2@\text{SnO}_2$  (0.1MS, 0.2MS, 0.3MS, 0.4MS) as a cathode, Zn foil as an anode, GF/A glass microfibre filter as a separator, graphite foil as a current collector, and 2M  $\text{ZnSO}_4 + 0.5\text{M MnSO}_4$  as the electrolyte comprised the completed battery.

As illustrated in Figure 3.1, the batteries were made as a CR2025 cell, which contains the top cap, cone spring, spacer, negative electrode, separator, positive electrode, and bottom cap. Around 0.5 ml of electrolyte was dumped into the separator during assembly of the component. A crimping machine was then used to shut the cell with a pressure of roughly 1  $\text{ton}/\text{cm}^2$ .

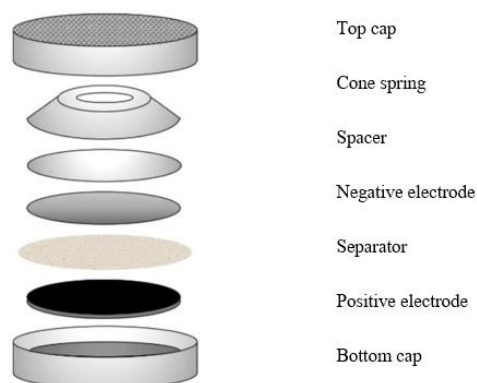


**Figure 3.1** The components of a CR2025 battery test cell.

### 3.3.2 Pouch cell

To fabricate the working electrode, a slurry was made in the same way as for the CR2025 coin cell type, but with a current collector of 0.10 mm graphite sheet. The electrode was then coated with 25  $\mu\text{m}$  thickness on a graphite sheet using a doctor blade machine. Next, the solvent was then removed by drying it under vacuum. The positive electrode sheet was finally obtained with a size of 3.8\*7.5 cm, the sheet was cut into a rectangle.

When fabricating the battery, pouch cells were used in the battery's construction. Aluminum laminated film, a composite  $\text{MnO}_2$  or  $\text{MnO}_2@\text{SnO}_2$  (0.3MS) as a cathode, GF/A glass microfiber filter as a separator, Zn foil as an anode, graphite foil as a current collector, and 2M  $\text{ZnSO}_4$  as the electrolyte were employed in roughly 15 ml of the completed battery. After that, a sealer at a temperature of 175  $^\circ\text{C}$  was used to shut the cell.



*Figure 3.2 The components of a pouch cell battery.*

### 3.4 Positive Electrode characterizations

#### 3.4.1 Structural properties

The crystal structure of synthesized samples was confirmed by powder X-ray diffraction (XRD) using  $\text{CuK}\alpha$  radiation. To check the correctness of the structure and the composition of manganese oxide from synthesis to match the desired one.

#### 3.4.2 Morphology

The morphology of samples was analyzed using a field-emission scanning electron microscope (FE-SEM). FE-SEM characterizations of pristine  $\text{MnO}_2$  electrodes and  $\text{MnO}_2@\text{SnO}_2$  (0.1MS, 0.2MS, 0.3MS and 0.4MS) were carried out to clearly see the increased component of the  $\text{SnO}_2$ -coating layer.

#### 3.4.3 Chemical composition

An energy dispersive X-ray (EDX) linked to the FE-SEM was used to examine the element distribution of the samples, revealing a uniform distribution of Mn, O, Sn across for  $\text{MnO}_2@\text{SnO}_2$  electrode surface, confirming the presence of  $\text{SnO}_2$

### 3.5 Electrochemical Techniques

#### 3.5.1 Battery Performance

A battery analyzer was used to measure the battery galvanostatic charge-discharge cycle. Within the voltage range of 1.0-1.75 V, the rate performance of pristine  $\text{MnO}_2$  electrodes and  $\text{MnO}_2@\text{SnO}_2$  (0.1MS, 0.2MS, 0.3MS and 0.4MS) electrode was investigated. Coin cells were tested for 10 cycles at various current densities (100, 200, 300, and 400  $\text{mA g}^{-1}$ ) to investigate rate performance. Following that, 60 more cycles were run continuously to check cycling stability at a current density of 100  $\text{mA g}^{-1}$ . Electrochemical testing was carried out at a room temperature of 25 °C.

### 3.5.2 Cyclic voltammetry (CV)

To get insight into the reaction kinetics of pristine  $\text{MnO}_2$  electrodes and  $\text{MnO}_2@\text{SnO}_2$  (0.1MS, 0.2MS, 0.3MS, 0.4MS) electrodes in ZIBs, cyclic voltammetry measurements were done at various potential scan speeds. The CV of pristine  $\text{MnO}_2$  electrodes and  $\text{MnO}_2@\text{SnO}_2$  (0.1MS, 0.2MS, 0.3MS, 0.4MS) electrodes was determined using a battery analyzer with a voltage range of 1.0-1.85 V (vs.  $\text{Zn}^{2+}/\text{Zn}$ ) at a scan rate of  $0.1 \text{ mVs}^{-1}$ . Electrochemical testing was carried out at a room temperature of  $25 \text{ }^\circ\text{C}$ .

### 3.5.3 Electrochemical Impedance Spectroscopy (EIS)

To gain a better understanding of the reaction kinetics, electrochemical impedance spectroscopy (EIS) measurements were taken at various potentials during the discharge process of pristine  $\text{MnO}_2$  electrodes and  $\text{MnO}_2@\text{SnO}_2$  (0.1MS, 0.2MS, 0.3MS, 0.4MS) electrodes.

Electrochemical Impedance Spectroscopy (EIS) of the battery was measured using a battery analyzer. EIS of the pristine  $\text{MnO}_2$  electrodes and  $\text{MnO}_2@\text{SnO}_2$  (0.1MS, 0.2MS, 0.3MS, 0.4MS) electrode was conducted in a frequency range of 100 kHz to 10 mHz with a voltage amplitude of 5 mV. Electrochemical testing was carried out at a room temperature of  $25 \text{ }^\circ\text{C}$ .

### 3.6 Inductively Coupled Plasma (ICP) [20]

Inductively Coupled Plasma (ICP) is used to detect metals and several non-metals in liquid samples at very low concentrations. It can be used to determine the amount of manganese ion dissolved in the electrolyte. After the galvanostatic charge/discharge cycling test is completed at 20, 40, 60, 80 and 100 cycles, the electrolyte is extracted from the pouch cell battery test. In order to compare the results, the systems with pristine  $\text{MnO}_2$  electrodes and  $\text{MnO}_2@\text{SnO}_2$  (0.3MS) electrode were measured.

### 3.7 Methodology

In this research, the experiment was divided into 4 parts as shown in figure 3.3.

Part I is manganese oxide synthesis according to section 3.2.1 and structural properties study according to section 3.4.

Part II is the synthesis of manganese oxide coated with tin oxide in different proportions, i.e., 0.1, 0.2, 0.3 and 0.4 g  $\text{SnCl}_2 \cdot 2\text{H}_2\text{O}$  according to section 3.2.2, and the structural properties of section 3.4 are studied.

Part III is the fabrication of a working electrode using manganese oxide (from part I) and manganese dioxide coated with tin oxide (from part II). It is composed by the Doctor blade machine method and studied the morphology and chemical composition of the electrode. Electrochemical measurements were used to verify the functionality of pristine manganese dioxide electrodes and manganese dioxide coated with tin oxide according to section 3.5 and to study the effect of tin oxide coating with different proportions. The one with optimal properties was chosen to be positive electrode for further study.

Part IV is the study of the properties of the electrode in terms of the dissolution of manganese as an electrolyte with the Inductively Couple Plasma (ICP) test.

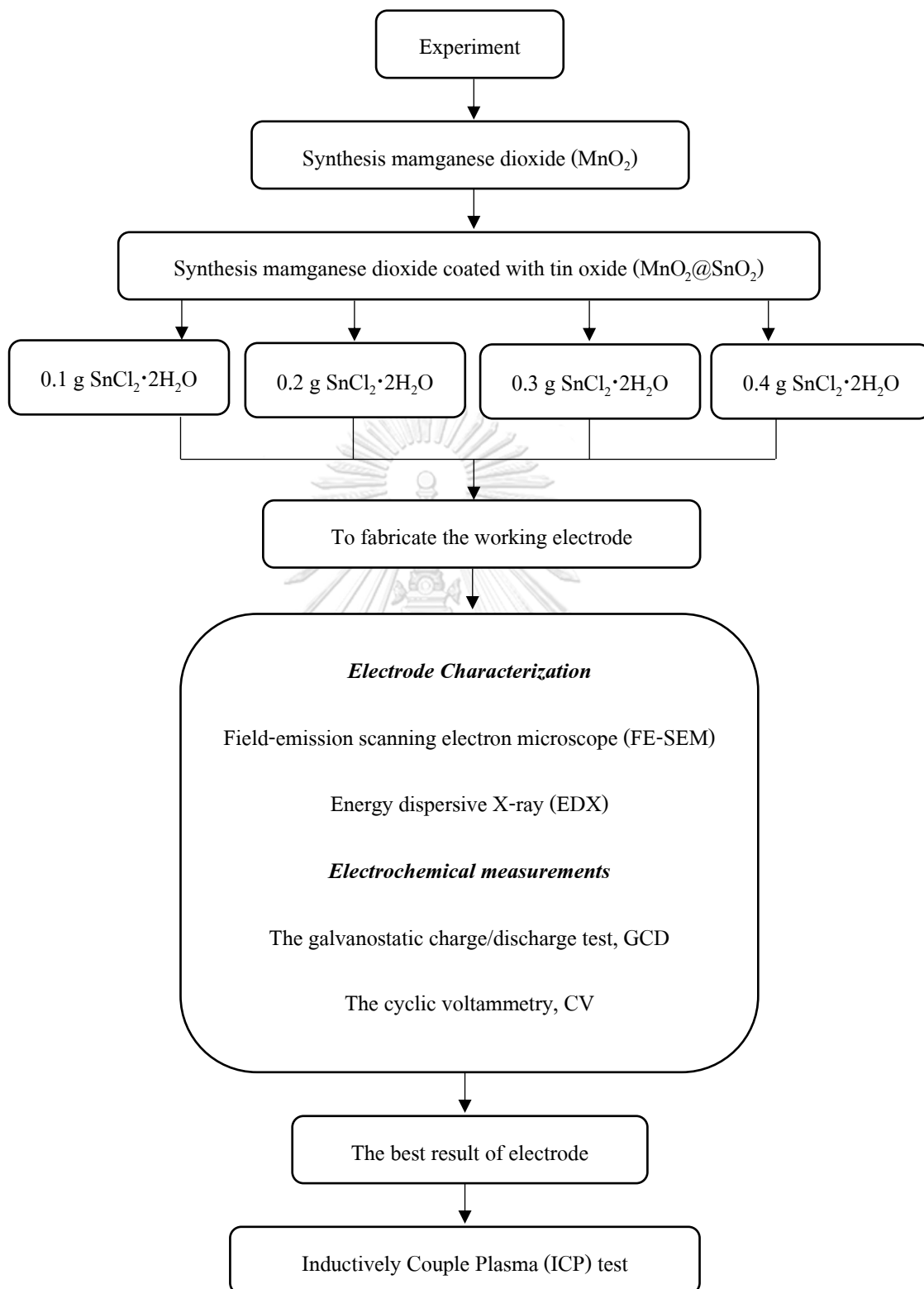


**Figure 3.3** Methodology of this research.



## CHAPTER 4

### RESULTS AND DISCUSSION

#### 4.1 Materials Characterization

Tin oxide coated onto manganese dioxide ( $\text{MnO}_2@\text{SnO}_2$ ) was prepared using wet-chemical approach. To verify the presence of the  $\text{SnO}_2$  layer on the  $\text{MnO}_2$  surface, we first performed X-ray diffraction (XRD) on two respective samples, pristine  $\text{MnO}_2$  (Figure 4.1) and  $\text{MnO}_2@\text{SnO}_2$  (Figure 4.2). For both pristine  $\text{MnO}_2$  and  $\text{MnO}_2@\text{SnO}_2$ , the main diffraction peaks observed at  $2\theta = 12.784^\circ, 18.108^\circ, 28.842^\circ, 37.523^\circ, 41.969^\circ, 49.865^\circ, 56.373^\circ, 60.276^\circ, 65.110^\circ, 69.713^\circ, 72.714^\circ$  were attributed to the (110), (200), (220), (211), (301), (411), (600), (521), (002), (541) and (321) face, respectively. All the peaks were in good agreement with the standard card reflections of manganese dioxide. All the diffraction peaks of  $\text{MnO}_2$  are well assigned to the  $\text{MnO}_2$  (PDF 00-044-0141).

Figure 4.2 presents the XRD patterns of  $\text{MnO}_2@\text{SnO}_2$  microparticle, the main diffraction peaks observed at  $2\theta = 26.701^\circ, 34.390^\circ, 38.119^\circ, 39.475^\circ, 42.827^\circ$  and  $52.270^\circ$  are observed corresponding to the  $\text{SnO}_2$  coating (PDF 01-079-6887). No additional peaks for other phases are detected, demonstrating a high purity of the  $\text{MnO}_2@\text{SnO}_2$  microparticle. This confirms that our  $\text{SnO}_2$  coating method does not affect the bulk structure, and the predominant phase present is  $\text{MnO}_2$ .

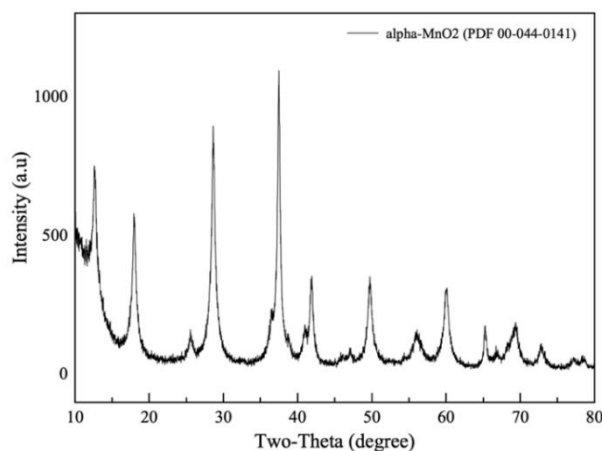


**Figure 4.1** XRD patterns of the  $\alpha\text{-MnO}_2$  nanoparticle.

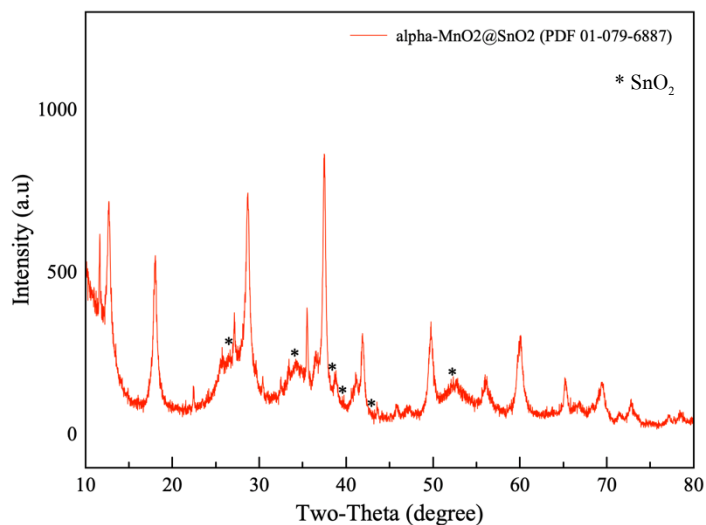


**Figure 4.2** XRD patterns of the  $\alpha\text{-MnO}_2\text{@SnO}_2$  nanoparticle.

Energy-distributed X-ray mapping (EDX) analyzes continue to confirm the composition of the composite material and the mapping images indicate that the elements are distributed throughout the structure. As shown in Figure 4.3(a-e), the composite nanoparticles consisted of Mn, O, Sn elements and the elements were well distributed.

Field emission scanning electron microscopy (FE-SEM) was used to characterize the morphology of tin oxide grown on manganese dioxide. The FE-SEM image of the pristine manganese dioxide as shown in Figure 4.4(a-b) and the FE-SEM images of the  $\text{MnO}_2\text{@SnO}_2$  composite are shown in Figure 4.4(c-f), tin oxide flakes can be seen to grow and cover the surface of manganese dioxide flakes in a layered manner. While using high magnification, the coarse layer covering the manganese dioxide structure is clearly visible. The morphology of the composite sample remained unchanged. It is covered with a layer of  $\text{SnO}_2$ , but the surface is extremely rough and streaky and the  $\text{SnO}_2$  density on  $\text{MnO}_2$  increased in proportion to the significant increase of  $\text{SnCl}_2\cdot 2\text{H}_2\text{O}$  for 0.1MS, 0.2MS, 0.3MS and 0.4MS positive electrodes (0.1, 0.2, 0.3 and 0.4 g  $\text{SnCl}_2\cdot 2\text{H}_2\text{O}$ , respectively). Such hierarchical  $\text{MnO}_2\text{@SnO}_2$  heterostructure indicates an increased reaction site and interface area between the electrode material and the electrolyte. Both of which allow this material to have a high specific capacity. In addition, the

branches of the  $\text{SnO}_2$  nanoparticles not only provide a high surface area for  $\text{Zn}^{2+}$  ion stripping/plating and structural flexibility for volume changes but also improve the electrical conductivity of the electrode which leads to better electrochemical efficiency [9, 20, 21]

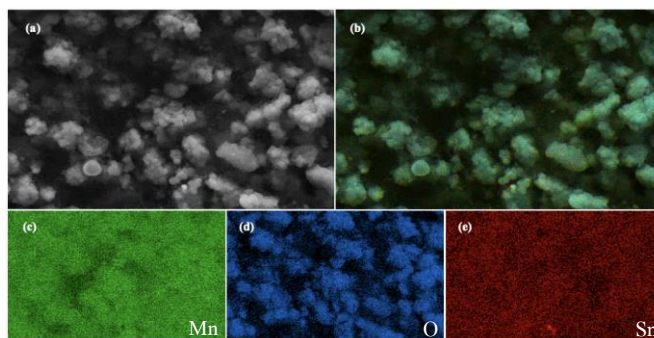


**Figure 4.3** EDX mapping of  $\text{MnO}_2@\text{SnO}_2$  electrode.

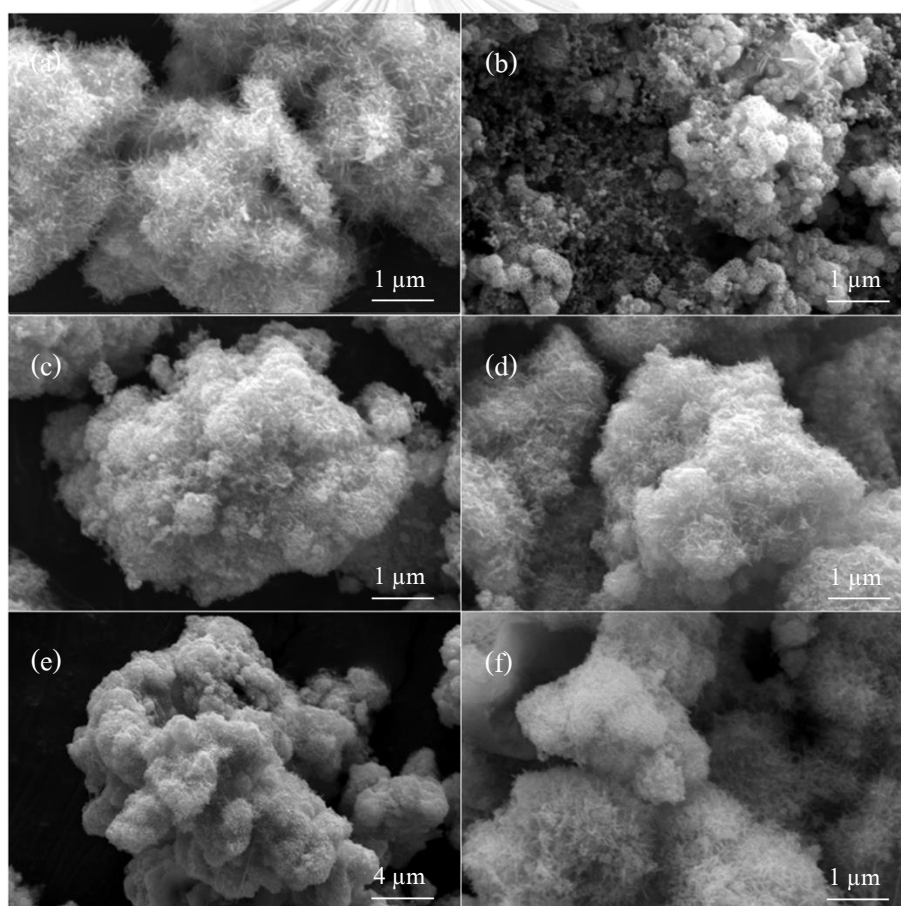


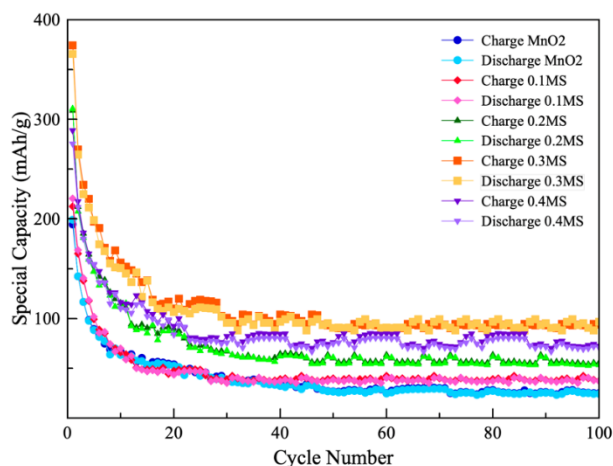
**Figure 4.4** FE-SEM images of (a)  $\text{MnO}_2$  nanoparticle (high magnification,  $\times 50000$ ), (b)  $\text{MnO}_2$  electrode (high magnification,  $\times 50000$ ) and (c-f)  $\text{MnO}_2@\text{SnO}_2$  nanoparticle (high magnification,  $\times 50000$ )

## 4.2 Electrochemical performance of batteries

To examine the effect of coating the SnO<sub>2</sub> layer with different proportions of SnCl<sub>2</sub>·2H<sub>2</sub>O used as a substrate for the formation of various SnO<sub>2</sub> layers on MnO<sub>2</sub> used as cathode for zinc ion batteries study of electrochemical performance specific charge/discharge capacities of positive electrodes with 0.1, 0.2, 0.3 and 0.4 g SnCl<sub>2</sub>·2H<sub>2</sub>O (hereinafter 0.1MS, 0.2MS, 0.3MS and 0.4MS, respectively) were plotted compared to the cycle number in use as shown in Figure 4.5.

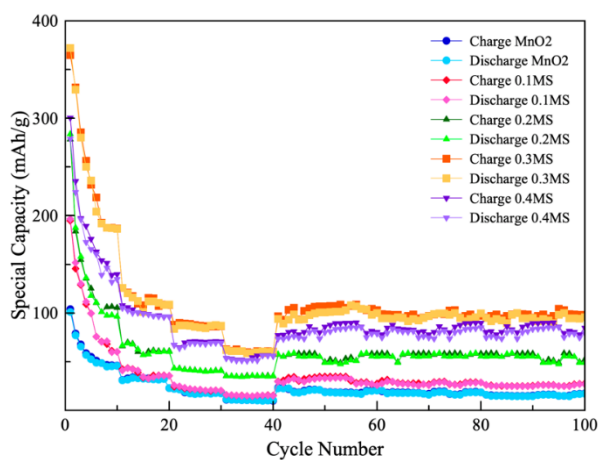
The results showed that all positive electrode capacitance gradually decrease as the cycle number increases. The battery's performance was analyzed with a constant current of 100 mAh/g. The initial discharge specific capacity of the pristine MnO<sub>2</sub> positive electrode was 199.02 mA g<sup>-1</sup> and remained 26.37 mAh g<sup>-1</sup> after 100 cycles, approximately 13.25%. The SnO<sub>2</sub>-coated electrode shows a very attractive battery performance, for 0.1MS positive electrode it has an initial capacity of 220.47 mAh g<sup>-1</sup> and it is still 40.68 mAh g<sup>-1</sup> after 100 cycles with 18.45% capacity retention. While the 0.2MS cathode has an initial capacity of 310.50 mAh g<sup>-1</sup> and remains at 61.60 mAh g<sup>-1</sup> after 100 cycles with a capacity of 19.8%. The 0.3MS positive electrode has a very outstanding initial capacity of 365.37 mAh g<sup>-1</sup> and the capacity remains at 99.44 mAh g<sup>-1</sup> after 100 cycles with 27.22% capacity retention, which is greater than the proportion of other electrodes processed with an SnO<sub>2</sub> layer coating and pristine MnO<sub>2</sub>. The 0.4MS positive electrode has an initial capacity of 275.44 mAh g<sup>-1</sup> and remained at 66.69 mAh g<sup>-1</sup> after 100 cycles with a capacity of 24.21%

This experiment indicated that the SnO<sub>2</sub> coating could greatly improve the rate efficiency. This may benefit from higher electrical conductivity and structural stability [9, 22], as is the SnO<sub>2</sub> coating on the electrode, which acts as an "artificial SEI" on the electrode surface to prevent electrolyte penetration and reduce side reactions [23, 24]. This results in stable cycling efficiency. It can be seen that the 0.3MS positive electrode treated with SnO<sub>2</sub> coating with a substrate fraction of 0.3 g SnCl<sub>2</sub>·2H<sub>2</sub>O has an outstanding initial capacitance. It also shows the best capacity to maintain battery capacity in comparison with the pristine MnO<sub>2</sub> and MnO<sub>2</sub>@SnO<sub>2</sub> with different SnO<sub>2</sub> layer formation.



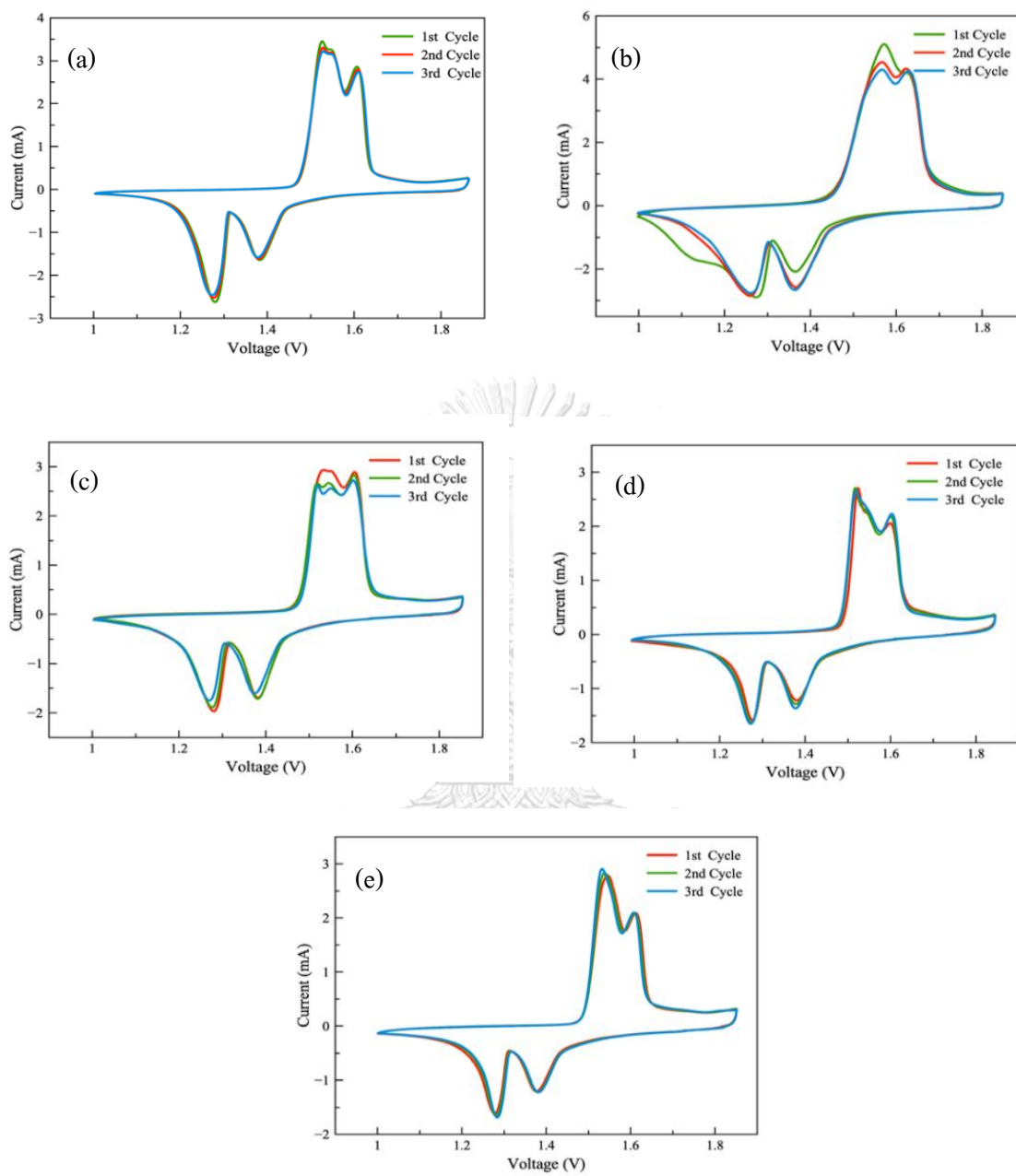
**Figure 4.5** Cycle performance of MnO<sub>2</sub>, 0.1MS, 0.2MS, 0.3MS and 0.4MS electrodes at current rate 100 mA g<sup>-1</sup>.

Figure 4.6 shows a comparison of the discharging specific capacitance at the following rates: 0.1, 0.2, 0.3 and 0.4 A g<sup>-1</sup> for an electrode with a positive electrode 0.1MS, 0.2MS, 0.3MS and 0.4MS. The specific discharge capacity will gradually decrease with increasing current rate from 0.1 to 0.4 A g<sup>-1</sup>. For positive electrodes 0.3MS, it provided an active discharge specific capacity this is higher than electrodes processed with other positive electrodes at any rate. The pristine MnO<sub>2</sub> positive electrode provides a comparatively lower specific discharge capacity with all four electrodes (0.1MS, 0.2MS, 0.3MS and 0.4MS) at all rates.



**Figure 4.6** Rate capability as a function of the current rate (100, 200, 300 and 400 mA g<sup>-1</sup>) of MnO<sub>2</sub>, 0.1MS, 0.2MS, 0.3MS and 0.4MS electrodes.

To assess electrochemical reactions and mechanisms that enhance battery performance, cyclic voltammetry (CV) and electrochemical impedance spectroscopy (EIS) were studied. Positive electrode voltammogram circuits with 0.1MS, 0.2MS, 0.3MS, 0.4MS at a voltage range of 1.0 - 1.85 V were performed and a scan rate of 0.1 mV/s as shown in Figure 4.7. The CV profile can indicate the electrochemical reaction, where reduction peak is a discharging process and oxidation is a charge process. All positive electrodes show a similar voltammetric cycle curve, where the first three cycles of 0.1MS, 0.2MS, 0.3MS and 0.4MS electrodes are shown in figure 25(b-e) respectively. Peak and shape are identical to that of pristine MnO<sub>2</sub> as shown in figure 25(a), indicating that the SnO<sub>2</sub> coating does not change the redox reaction of the pristine electrode [26,28-29]. By the reduction process of the pristine MnO<sub>2</sub> electrode, there were two peaks of 1.28 V and 1.38 V. There are two oxidation apparent peaks set at 1.53 V and 1.61 V, proving a two-stage reaction during the discharge/charge process for the pristine MnO<sub>2</sub> electrode, while the 0.1MS and 0.4MS positive electrode reduction process has two reduction peaks of 1.27 V, 1.36 V and 1.27 V, 1.37 V, respectively. There are two oxidation apparent peaks located at 1.58 V, 1.63 V and 1.55 V, 1.61 V, respectively. The cyclic curve confirms that the redox reaction occurs in the range of (1.0 - 1.85 V), which has similar voltammetric cycle curves. While the 0.2MS and 0.3MS positive electrodes show the reduction process, there are two peaks of 1.29 V, 1.38 V and 1.27 V, 1.38 V, respectively. There are three distinct peaks for the oxidation process, located at 1.50 V, 1.55 V, 1.61 V and 1.52 V, 1.54 V, 1.60 V, respectively, indicating that the mass transfer of the electrode is changed from the electrode. The 0.2MS and 0.3MS positive electrode may be the result of the formation of an SnO<sub>2</sub> layer on the surface of MnO<sub>2</sub> but at the same time the voltammetric cycle curve for the 0.3MS electrode shows the stable in mass transfer when the battery is used repeatedly, its characteristics and mass transfer capacity are uniform. With the pristine MnO<sub>2</sub> electrodes with repeated use the mass transfer capacity will gradually decrease with use in the next cycle.



**Figure 4.7** Cyclic voltammetry (CV) curves of (a)  $\text{MnO}_2$ , (b) 0.1MS, (c) 0.2MS, (d) 0.3MS and (e) 0.4MS electrodes at scan rate of  $0.1 \text{ mV s}^{-1}$ .

Considering the shape of the CV curve, the presence of an SnO<sub>2</sub> layer coated onto the surface of the MnO<sub>2</sub> results in a high surface area. This increases the stripping/plating area of the Zn<sup>2+</sup> ions, which can be observed from the SnO<sub>2</sub>-coated electrode CV curve has a plumper curve than CV curve of pristine MnO<sub>2</sub> as shown in figure 4.7. The charge behavior of SnO<sub>2</sub> coated electrodes results in better battery performance. Consistent with the above results, the battery efficiency from the charging/discharging experiment of the battery will be better after the SnO<sub>2</sub> coating is applied to the surface of the MnO<sub>2</sub>. Obviously, the diffusion of Zn<sup>2+</sup> ions in the MnO<sub>2</sub> layer and electron transport affect the rate of charge/discharge process. In this case, because the surface-covered SnO<sub>2</sub> has much higher electrical conductivity than MnO<sub>2</sub>, it serves to facilitate the rapid electron transport. These characteristics make it an advantage for electrodes that are coated with an SnO<sub>2</sub> layer.

To study diffusion dynamics, Nyquist plots show the transformation with various charge/discharge conditions. For the pristine MnO<sub>2</sub>, 0.1MS, 0.2MS, 0.3MS and 0.4MS positive electrode in Figure 4.8(a-e) shows a comparison between the new battery and the battery after various positive electrode charge/discharge tests. It was tested under the same conditions before and after charge/discharge at frequencies from 100 kHz to 0.01 Hz at open circuit potential. It was found that in the pristine MnO<sub>2</sub> positive electrodes, 0.1MS, 0.2MS, 0.3MS and 0.4MS reduced both charge transfer and SEI resistance when these batteries were tested for 100 charge/discharge cycles.

When considering the Nyquist diagram for the after-charge/discharge electrode (Figure 4.8f), the pristine MnO<sub>2</sub> and 0.1MS positive electrodes are somewhat similar in shape with a semicircle at high frequencies and a straight line in the low frequency which appears only a single semicircular at high frequencies which indicates that the contact between the electrolyte and the positive electrode surface. The radius of the semicircle in the high to medium frequency region for the 0.1MS positive electrode is clear. The 0.1MS electrode is much smaller than the radius of the pristine MnO<sub>2</sub> electrode, indicating that the charge transfer resistance at the interface in the pristine MnO<sub>2</sub> is less than 0.1MS electrode. This indicates that the transfer of Zn<sup>2+</sup> ions in the

0.1MS electrode can improve electron transfer efficiency. In contrast, the Nyquist diagram for 0.2MS, 0.3MS and 0.4MS positive electrodes after charge/discharge was tested at frequencies from 100 kHz to 0.01 Hz, showing a semicircle two bands at high and medium frequencies which indicates the charge transfer resistance and the resistivity of the interphase solid electrolyte (SEI) film layer, respectively which may be due to the formation of an  $\text{SnO}_2$  layer on the surface of  $\text{MnO}_2$ , which acts as an SEI film, preventing direct contact between the electrode and electrolyte, thus helping for battery performance for longer use [17].

Additionally, Bode plot in Figure 4.9(a-j) shows a similar trend to the Nyquist diagram, in which there is an apparent single phase angle shift of the pristine  $\text{MnO}_2$  electrode and 0.1MS, while the 0.2MS, 0.3MS and 0.4MS electrode have two-phase angle shift. This is shown at the high and medium frequency region, followed by an inclined ( $\sim 45^\circ$ ) line at the low frequency region caused by the Warburg-type impedance of the host structure ( $W_{\text{mt}}$ ) transport, electrolyte resistance ( $R_e$ ), solid electrolyte interphase resistance ( $R_{\text{SEI}}$ ) and charge transfer resistance ( $R_{\text{ct}}$ ) (details are given in the table in the appendix).

The  $\text{Zn}^{2+}$  ion diffusion phenomenon (Warburg resistance) on the positive electrode at low frequencies, the value decreases after it is used. This same behavior was shown for all electrodes. The Warburg resistance could be explained by an initial electrochemical grinding, increasing the surface area of active materials. This improves the active material surface area and shows how stably  $\text{Zn}^{2+}$  ions can be transferred into the  $\text{MnO}_2$  structure, the lower the Warburg resistance is, the better the insertion of Zn ions be. This directly affects the performance of the battery. Thus, having the 0.3MS electrode showing the lowest Warburg resistance value is consistent with the best battery performance test results (details are given in the table in the appendix). This is because it has the best ability to transfer  $\text{Zn}^{2+}$  ions in/out the  $\text{MnO}_2$  structure.

In order to deeply examine the reasons for the circuit performance and capacity rating of pristine  $\text{MnO}_2$  and 0.1MS, 0.2MS, 0.3MS and 0.4MS positive electrode using the technique FE-SEM to observe the physical characteristics of the positive electrodes with different proportions of  $\text{SnO}_2$  before and after 100 charge/discharge cycles, which were disassembled from the battery and dried prior to testing, as shown in Figure 4.10(a-j).

To confirm the protection of the  $\text{MnO}_2$  structure from the  $\text{SnO}_2$  coating for the 0.1MS, 0.2MS, 0.3MS and 0.4MS positive electrode, the results are presented as seen from figure 4.10a. The surface morphology of the electrode through  $\text{MnO}_2$  before cycling, the surface characteristics and distribution of  $\text{MnO}_2$  were relatively uniform. As shown in figure 4.10f, clear cracks and holes were observed in the  $\text{MnO}_2$  electrode after cycling. This is a result of the large change in volume and dissolution of  $\text{MnO}_2$  during charging/discharging. In comparison, it can be identified in the positive electrode 0.1MS, 0.2MS, 0.3MS and 0.4MS as shown in figure 28(b-e) of before the cycling test and figure 4.10(g-j) of after cycles. There is a slight crack on the surface of the electrode, but the appearance is a smooth and consistent surface with no cracks or large holes. This indicates the structural stability of  $\text{SnO}_2$  and contributes to the protection of  $\text{MnO}_2$  nanoparticle morphology. The presence of  $\text{SnO}_2$  can act as a physical barrier layer to avoid the solubility formed by the contact between manganese oxide and the electrolyte and may mitigate the volume expansion of  $\text{MnO}_2$ , thereby greatly improving the cycle stability of  $\text{MnO}_2$  during charging and discharging.

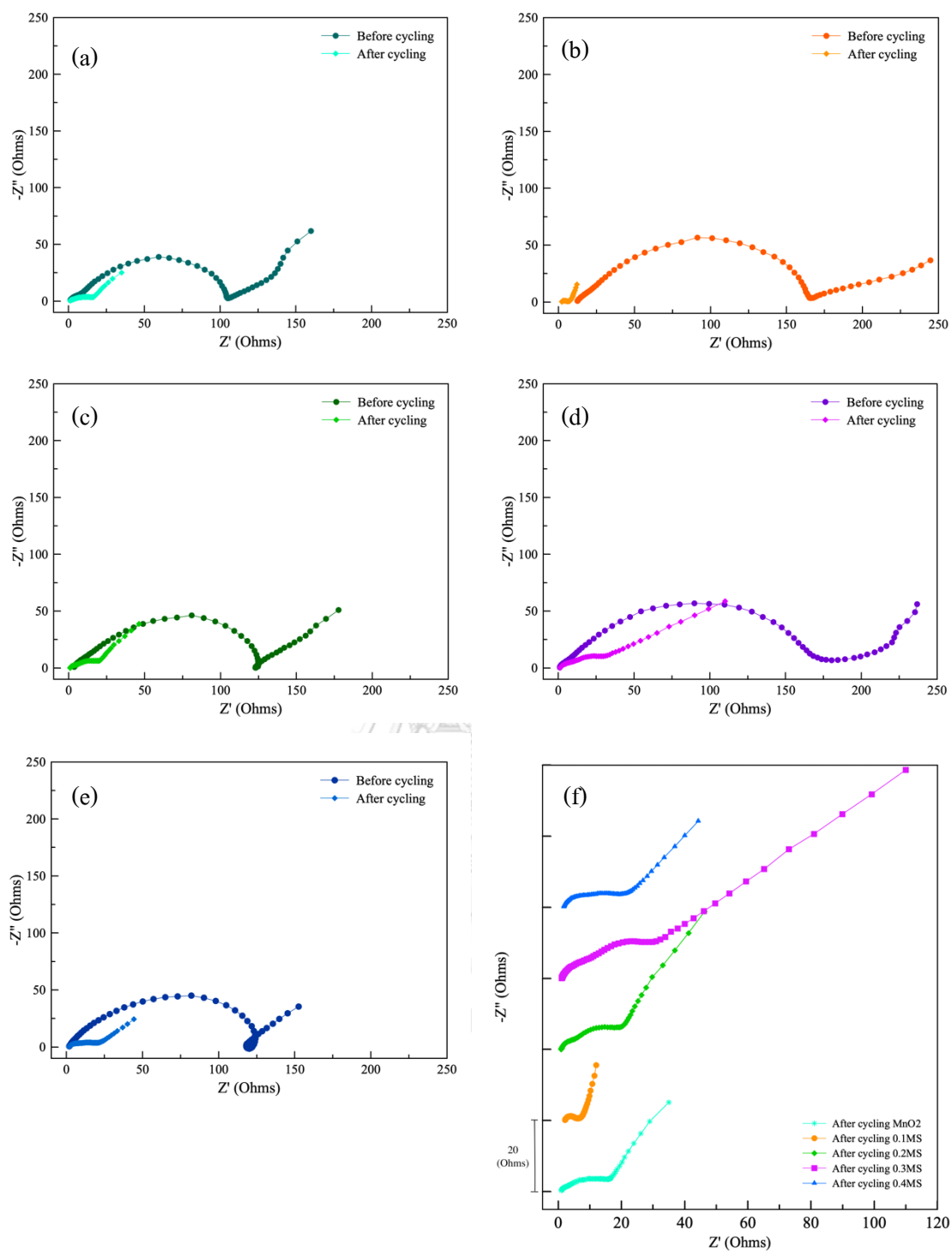


**Figure 4.8** Nyquist plots of the positive electrode with (a) MnO<sub>2</sub>, (b) 0.1MS, (c) 0.2MS, (d) 0.3MS and (e) 0.4MS electrodes of fresh batteries and after 100 cycles (f) Nyquist plot comparing of after cycling at each electrode.

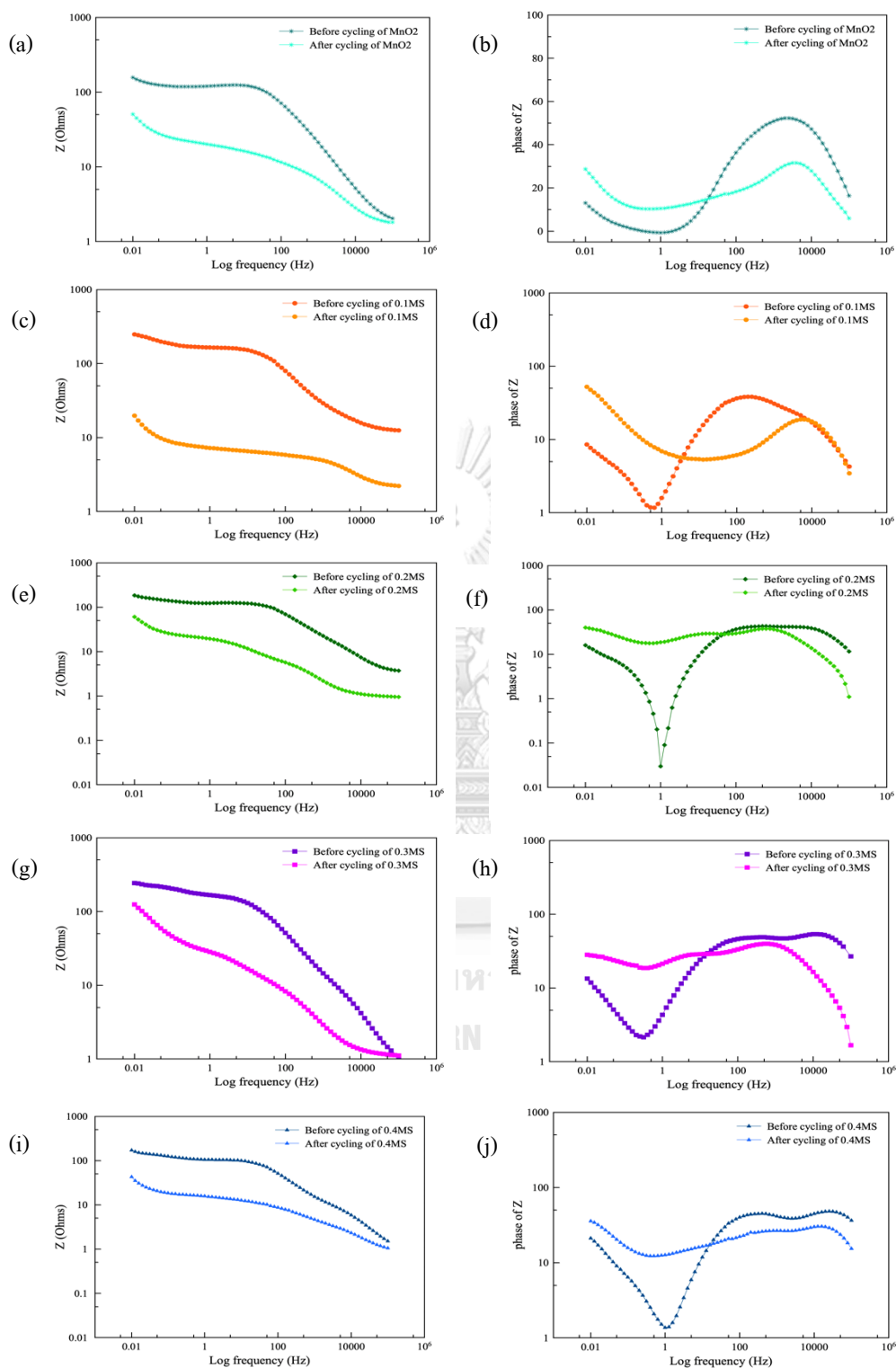


**Figure 4.9** Bode plots of the positive electrode with with (a, b)  $\text{MnO}_2$ , (c, d) 0.1MS, (e, f) 0.2MS, (g, h) 0.3MS and (i, j) 0.4MS electrodes.

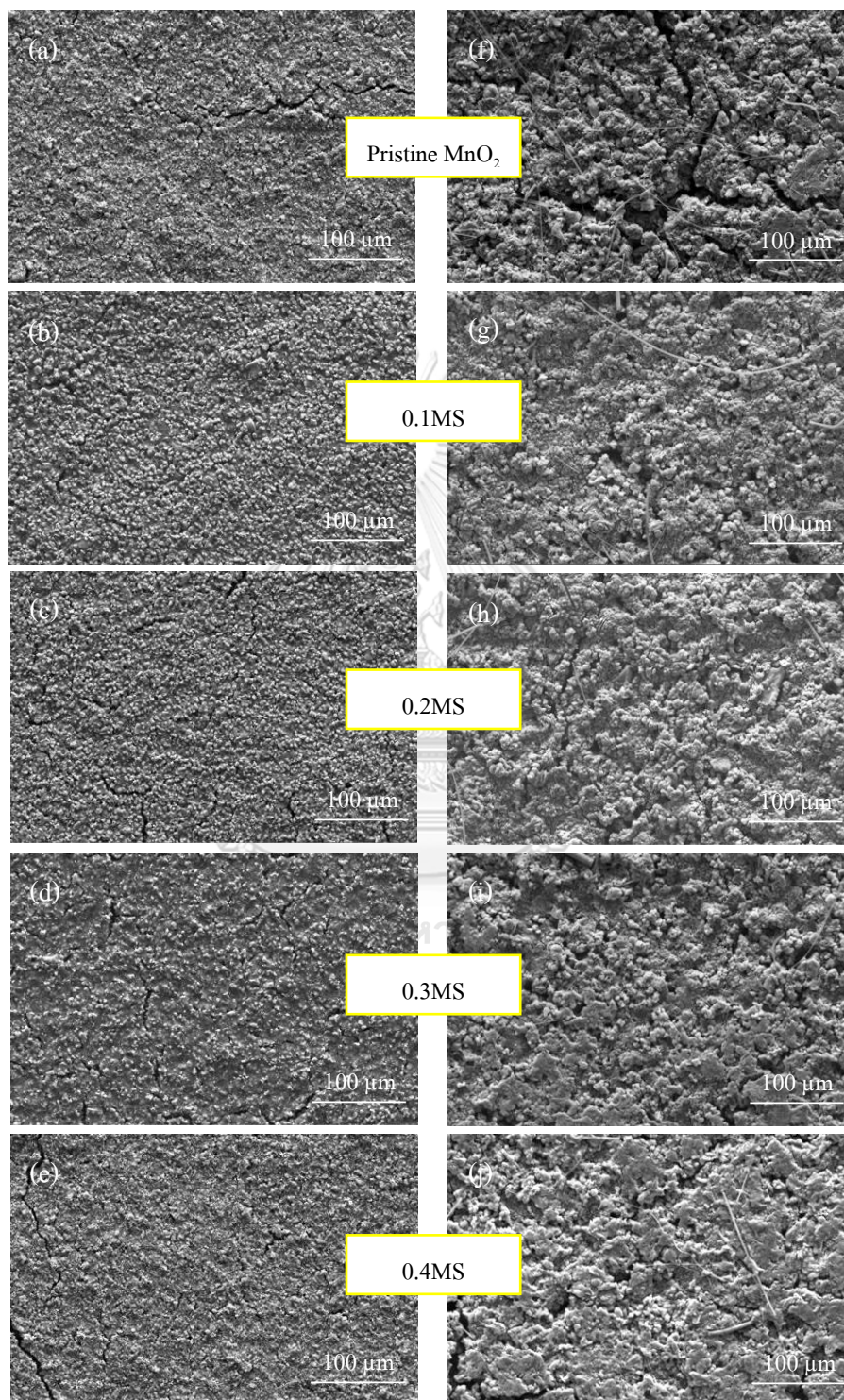


**Figure 4.10** FE-SEM image of positive electrode processed with MnO<sub>2</sub>, 0.1MS, 0.2MS, 0.3MS and 0.4MS electrodes (a, b, c, d, e) before the cycling test and (f, g, h, i, j) after 100 cycles.

To understand the causes of rapid fading in pristine  $\text{MnO}_2$ , ICP measurement was performed to determine the electrolyte composition during cycling. Here, pouch cells were invented (details are shown in the experiment section 3.6) as shown in figure 4.11a. A charge/discharge test was then performed at  $100 \text{ mA g}^{-1}$ . After that, the electrolytes in these cells were collected for testing after cycling at 20, 40, 60, 80 and 100 cycles as shown in figure 4.11b. The manganese concentration in the case of the pristine  $\text{MnO}_2$  is high as shown in figure 4.12. This indicates that manganese corrosion is exacerbated by direct contact between the active materials. For  $\text{MnO}_2$  comparison, the 0.3MS  $\text{SnO}_2$ -coated cathode is hereby selected for testing. This is because 0.3MS positive electrode has electrochemical efficiency and shows better stability in maintaining battery capacity than other positive electrodes. It can be seen that the 0.3MS positive electrode has much less manganese solubility. This corresponds to better performance at low current densities.



**Figure 4.11** (a) Pouch cell of the Zinc- $\text{MnO}_2$  and Zinc- $\text{MnO}_2@/\text{SnO}_2$  (0.3MS) batteries with positive electrode processed, (b) Electrolytes solution from pouch cell after charge/discharge 20, 40, 60, 80 and 100 cycles,

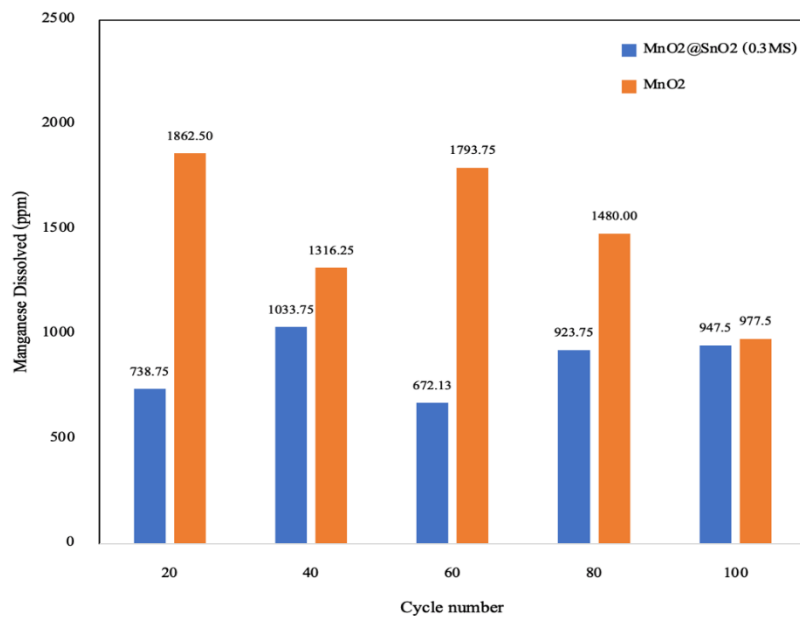


*Figure 4.12 ICP results after different numbers of cycles.*



## CHAPTER 5

### CONCLUSION

In this work, the surface treatment of manganese dioxide electrodes by tin oxide coating by wet-chemical method was studied, comparing the pristine manganese dioxide electrodes. The study revealed a uniform distribution of the elements Mn, O and Sn on the  $\text{MnO}_2@\text{SnO}_2$  electrode. It was found that the  $\text{SnO}_2$  cover increased in proportion to the initial increase in the reactant. From 0.1 to 0.4 g  $\text{SnCl}_2 \cdot 2\text{H}_2\text{O}$ , the electrical performance study showed that the improved electrodes of 0.1MS, 0.2MS, 0.3MS and 0.4MS were stable in battery operation and showed better operating capacity than pristine manganese electrodes after 100 cycles of use. Initial specific discharge capacity of 0.1MS, 0.2MS, 0.3MS and 0.4MS positive electrodes at the rate current of  $100 \text{ mA g}^{-1}$  is  $220.47 \text{ mAh g}^{-1}$ ,  $310.50 \text{ mAh g}^{-1}$ ,  $365.37 \text{ mAh g}^{-1}$  and  $275.44 \text{ mAh/g}$ , respectively. It can be observed that the 0.3MS positive electrode can discharge maximum specific charge. It also has high-rate capability and low self-discharge rate. Meanwhile the specific discharge capacity and specific capacity retention of the pristine  $\text{MnO}_2$  positive electrode is  $199.02 \text{ mAh g}^{-1}$ . The CV and EIS results revealed that the  $\text{SnO}_2$  coating greatly increased the zinc ion diffusion coefficient. In addition, the investigation revealed that  $\text{SnO}_2$  greatly increased the conductivity.

In addition, this 0.3MS positive electrode was able to reduce the solubility of manganese into the electrolyte better than the  $\text{MnO}_2$  positive electrode, in which it was confirmed by ICP test of the electrolyte after the test cycles.

## APPENDIX

**Bode plot of positive electrode**

Impedance of pristine MnO<sub>2</sub> electrode and MnO<sub>2</sub>@SnO<sub>2</sub> electrode (0.1MS, 0.2MS, 0.3MS and 0.4MS) before/after cycling.

$R_b$ : Bulk resistance of the cell (electrolyte, separator and electrode)

$R_{SEI}$ : Resistance of the interfacial layer

$R_{ct}$ : Charge-transfer resistance

W: Diffusional effects of zinc-ion on the host material

Before/ After	$R_b$	$R_{SEI}$	$R_{ct}$	W
<b>MnO2</b>	8.48/0.0156	96.0/1.04	194.0/12.7	17.6/6.68
<b>0.1MS</b>	2.37/0.0746	29.6/0.893	129.0/3.71	12.5/3.63
<b>0.2MS</b>	12.6/0.579	46.6/4.70	59.7/9.35	15.5/12.0
<b>0.3MS</b>	4.32/7.20	12.8/27.0	160.0/154.0	16.4/0.0589
<b>0.4MS</b>	25.1/0.0829	32.3/5.81	59.4/12.4	8.79/6.81



จุฬาลงกรณ์มหาวิทยาลัย  
**CHULALONGKORN UNIVERSITY**

## REFERENCES

1. Shang, H., et al., *MnO<sub>2</sub>@V<sub>2</sub>O<sub>5</sub> microspheres as cathode materials for high performance aqueous rechargeable Zn-ion battery*. Journal of Electroanalytical Chemistry, 2021. **890**: p. 115253.
2. Yang, B., et al., *Manganese oxides hierarchical microspheres as cathode material for high-performance aqueous zinc-ion batteries*. Electrochimica Acta, 2021. **385**: p. 138447.
3. Guo, J., et al., *Artificial solid electrolyte interphase for suppressing surface reactions and cathode dissolution in aqueous zinc ion batteries*. ACS Energy Letters, 2019. **4**(12): p. 2776-2781.
4. Yoon, S.Y. and B.J. Choi, *Electrical characteristics of tin oxide films grown by thermal atomic layer deposition*. Archives of Metallurgy and Materials, 2020. **65**.
5. He, H., et al., *Highly stable Zn metal anodes enabled by atomic layer deposited Al<sub>2</sub>O<sub>3</sub> coating for aqueous zinc-ion batteries*. Journal of materials chemistry A, 2020. **8**(16): p. 7836-7846.
6. Li, C., et al., *Cathode materials for rechargeable zinc-ion batteries: From synthesis to mechanism and applications*. Journal of Power Sources, 2020. **449**: p. 227596.
7. Guo, X., et al., *Zn/MnO<sub>2</sub> battery chemistry with dissolution-deposition mechanism*. Materials Today Energy, 2020. **16**: p. 100396.
8. Qiu, C., et al., *The function of Mn<sup>2+</sup> additive in aqueous electrolyte for Zn/δ-MnO<sub>2</sub> battery*. Electrochimica Acta, 2020. **351**: p. 136445.
9. Guo, S., et al., *Cathode interfacial layer formation via in situ electrochemically charging in aqueous zinc-ion battery*. ACS nano, 2019. **13**(11): p. 13456-13464.
10. Gou, L., et al., *α-MnO<sub>2</sub>@In<sub>2</sub>O<sub>3</sub> nanotubes as cathode material for aqueous rechargeable Zn-ion battery with high electrochemical performance*. Journal of The Electrochemical Society, 2019. **166**(14): p. A3362.
11. Ramasamy, H.V., et al., *Atomic layer deposition of Al<sub>2</sub>O<sub>3</sub> on P<sub>2</sub>-Na<sub>0.5</sub>Mn<sub>0.5</sub>Co<sub>0.5</sub>O<sub>2</sub> as interfacial layer for high power sodium-ion batteries*. Journal of Colloid and Interface Science, 2020. **564**: p. 467-477.
12. Liu, Y., et al., *Interfacial engineering coupled valence tuning of MoO<sub>3</sub> cathode for high-*

- capacity and high-rate fiber-shaped zinc-ion batteries.* Small, 2020. **16**(11): p. 1907458.
13. Gong, S.H., et al., *Electrochemical Assessment of Highly Reversible SnO<sub>2</sub>-Coated Zn Metal Anodes Prepared Via Atomic Layer Deposition for Aqueous Zn-Ion Batteries.* Available at SSRN 4058096.
  14. Meng, X., *Atomic-scale surface modifications and novel electrode designs for high-performance sodium-ion batteries via atomic layer deposition.* Journal of Materials Chemistry A, 2017. **5**(21): p. 10127-10149.
  15. Jurng, S., et al., *Minimized metal dissolution from high-energy nickel cobalt manganese oxide cathodes with Al<sub>2</sub>O<sub>3</sub> coating and its effects on electrolyte decomposition on graphite anodes.* Journal of The Electrochemical Society, 2019. **166**(13): p. A2721.
  16. Model, P.C.V.M.U., *2450-EC or 2460-EC Electrochemistry Lab System.* SJ Electronics, 2016.
  17. Islam, S., et al., *Carbon-coated manganese dioxide nanoparticles and their enhanced electrochemical properties for zinc-ion battery applications.* Journal of Energy Chemistry, 2017. **26**(4): p. 815-819.
  18. Li, W., et al., *Synthesis of SnO<sub>2</sub>@ MnO<sub>2</sub>@ graphite nanosheet with high reversibility and stable structure as a high-performance anode material for lithium-ion batteries.* Ceramics International, 2021. **47**(23): p. 33405-33412.
  19. Jaikrajang, N., et al., *Impact of Binder Functional Groups on Controlling Chemical Reactions to Improve Stability of Rechargeable Zinc-Ion Batteries.* ACS Applied Energy Materials, 2021. **4**(7): p. 7138-7147.
  20. Chen, C., et al., *Al-Intercalated MnO<sub>2</sub> cathode with reversible phase transition for aqueous Zn-Ion batteries.* Chemical Engineering Journal, 2021. **422**: p. 130375.
  21. Liu, L., et al., *Alkali ions pre-intercalated layered MnO<sub>2</sub> nanosheet for zinc-ions storage.* Advanced Energy Materials, 2021. **11**(31): p. 2101287.
  22. Wu, B., et al., *Graphene scroll-coated  $\alpha$ -MnO<sub>2</sub> nanowires as high-performance cathode materials for aqueous Zn-ion battery.* Small, 2018. **14**(13): p. 1703850.
  23. Zhou, X., et al., *Exploring the interfacial chemistry between zinc anodes and aqueous electrolytes via an in situ visualized characterization system.* ACS Applied Materials & Interfaces, 2020. **12**(49): p. 55476-55482.

24. Lu, H., et al., *Engineering Al<sub>2</sub>O<sub>3</sub> atomic layer deposition: enhanced hard carbon-electrolyte interface towards practical sodium ion batteries*. Nano Energy, 2019. **64**: p. 103903.
25. Ramasamy, H.V., et al., *Atomic layer deposition of Al<sub>2</sub>O<sub>3</sub> on P2-Na<sub>0.5</sub>Mn<sub>0.5</sub>Co<sub>0.5</sub>O<sub>2</sub> as interfacial layer for high power sodium-ion batteries*. Journal of colloid and interface science, 2020. **564**: p. 467-477.
26. Yang, H., et al., *A New Hierarchical  $\alpha$ -MnO<sub>2</sub>-Nanotube@ SnO<sub>2</sub> Heterostructure as an Advanced Anode for High-Performance Lithium-Ion Batteries*. Journal of Nanoscience and Nanotechnology, 2018. **18**(11): p. 7811-7817.
27. Xue, X.-Y., et al., *SnO<sub>2</sub>/WO<sub>3</sub> core-shell nanorods and their high reversible capacity as lithium-ion battery anodes*. Nanotechnology, 2011. **22**(39): p. 395702.
28. Ni, Z., et al., *Tin doping manganese dioxide cathode materials with the improved stability for aqueous zinc-ion batteries*. Materials Chemistry and Physics, 2022: p. 126238.
29. Khamsanga, S., et al.,  *$\delta$ -MnO<sub>2</sub> nanoflower/graphite cathode for rechargeable aqueous zinc ion batteries*. Scientific reports, 2019. **9**(1): p. 1-9.

## VITA

**NAME** Nichakarn Meekaew

**DATE OF BIRTH** 23 Feb 1997

**PLACE OF BIRTH** Nakhon Si Thammarat, Thailand

**INSTITUTIONS ATTENDED** B.S Chemical Engineering Faculty of Engineering at Prince of Songkla University

**PUBLICATION** 7TH International Conference on recent advances in materials, minerals & environment (RAMM2022), 19-20 July 2022.  
Manganese dioxide coated with tin oxide as cathode material for high-performance aqueous zinc-ion battery.